

National University of Science and Technology
POLITEHNICA Bucharest
Faculty of Biotechnical Systems Engineering
Doctoral School of Biotechnical Systems Engineering
Domain: Environmental Engineering

DOCTORAL THESIS
SUMMARY
Monitoring CO_2 emissions from peri-urban wetlands in the context of climate change

Scientific Coordinator:
CSI Ph.D Habil. Dr. Eng.
DEÁK György

PhD Student:
ENACHE Natalia-Andreea

Keywords: CO_2 emissions, climate change, peri-urban wetlands, closed static chamber, closed dynamic chamber, EGM-5, Injection Kit, NbS, litter, biogeochemical modeling

CHAPTER 1. THE IMPORTANCE OF THEME. THE OBJECTIVES OF THE DOCTORAL THESIS.

The increase in the concentration of GHGs in the atmosphere causes the amplification of the effects of climate change over time. The accumulation of CO_2 in the atmosphere can be reduced through ecosystems, by accumulating CO_2 in vegetation and soil, thus creating the so-called carbon "pools" [1][2]. Soils and ecosystems in the wetlands store large amounts of C (carbon), which contribute to the reduction of CO_2, and the most important processes affecting the C balance of ecosystems are photosynthesis by surface vegetation, "soil and water respiration" in the case of wetlands. Wetland ecosystems are well known for their capacity to sequester and store C, primarily through the accumulation of OM (organic matter) under anaerobic conditions.

However, in this doctoral thesis, it was also investigated that wetlands release substantial amounts of CO_2 into the atmosphere through various biogeochemical processes, contributing to GHG emissions and climate change [3].

The case study area along the Dâmbovita River, located in the peri-urban area of Bucharest, offers the possibility of a detailed analysis of CO_2 emissions in a rapidly urbanizing region, especially at the transition between a riparian wetland ecosystem and the reservoir. The presence of robust aquatic and riparian vegetation in areas near the natural banks contrasts with the less dense vegetation in the transition section towards the city, providing a diverse dataset on how different vegetation densities affect CO_2 emissions. Furthermore, the PhD thesis aims to validate innovative methods for monitoring and estimating CO_2 fluxes, integrating static and dynamic closed chamber measurement methods with advanced mathematical statistical models, including numerical simulation. Due to the location of the study area in a peri-urban area, the results of the thesis make valuable contributions to preparing cities for the process of adapting to climate change and can be extended to other similar peri-urban areas, providing a replicable model of analysis and intervention.

The specific objectives are:

1. Analysis of CO_2 emissions from the soil-atmosphere and water-atmosphere interfaces through in-situ measurements and modeling methods.
2. Testing and validating innovative methods for determining CO_2 emissions from the water-atmosphere interface, emphasising their applicability in wetland ecosystems.
3. Identification and evaluation of the influence of meteorological factors (temperature, precipitation, wind speed, atmospheric pressure), as well as of the physico-chemical parameters of water and soil on CO_2 emissions.
4. Evaluation of the spatio-temporal variability of CO_2 emissions in the context of climate change.
5. Evaluation of the role of surface vegetation and litter on the ecosystem's capacity to capture and store C.
6. Validation of predictive models for estimating CO_2 emissions using values resulting from direct measurements.

7. Simulating the impact of climate change on CO_2 emissions in the case study area and assessing the ecosystem's capacity to act as a carbon sink, according to RCP 8.5

CHAPTER 2. CURRENT STATUS OF KNOWLEDGE REGARDING THE ANALYSIS OF CO_2 EMISSIONS FROM WETLAND ECOSYSTEMS IN THE CONTEXT OF CLIMATE CHANGE

2.1. The situation on the European level regarding the current state of wetlands in the context of climate change from a legislative point of view

In the current context of accelerated global climate change, which affects both present and future generations [4], international action has been initiated, and treaties and agreements have begun to be developed to limit and reduce GHG emissions. The EU (European Union) has made considerable efforts to mitigate climate change, improving environmental policy through a series of treaties, directives, and agreements that address these emissions, biodiversity loss, and environmental sustainability [5]. These European treaties and directives on climate change provide a comprehensive legal and policy framework that supports wetland conservation as a critical component of climate change mitigation and play a key role in the development of NbS, such as wetland conservation, which is an integral part of the global carbon cycle [2].

To limit the increase in GHG emissions, measures have been taken since 1992, when the world's nations signed the UNFCCC (United Nations Framework Convention on Climate Change) [6]. The UNFCCC sought to stabilize the concentration of GHGs in the atmosphere to allow ecosystems to adapt naturally to the impacts of climate change.

Since 1997, the Kyoto Protocol has imposed binding GHG reduction targets on developed signatory countries. The Protocol sets binding targets for industrialized countries to reduce GHG emissions [7]. In the first commitment period under the Kyoto Protocol (2008-2012), most EU Member States, including Romania, aimed to reduce greenhouse gas emissions by 8% compared to 1989. The second commitment period (2013-2020) was established by the "Doha Amendment", and the EU assumed a 20% reduction in emissions compared to 1990 [8].

Within the 21st Conference of the Parties to the United Nations Framework Convention on Climate Change (COP 21) in December 2015, the Paris Agreement was adopted, a legally binding and universally applicable instrument that guides global action to limit the increase in global average temperature to well below 2°C starting in 2021 [6].

The IPCC has developed a methodology for inventorying greenhouse gases from anthropogenic activities by key sectors [9][10]. These GHG inventories include the LULUCF sector, which covers emissions from forest ecosystems, agricultural land, grasslands, settlements, and other land, as well as wetland ecosystems [11]. The LULUCF Regulation (Regulation (EU) 2018/841) requires EU Member States to account for GHG emissions from land use, including wetlands, ensuring that these natural carbon sinks are conserved and enhanced [12].

These legislative efforts focus on halting the degradation and promoting the restoration of wetlands to support the carbon cycle and biodiversity, reinforcing the importance of wetlands in achieving climate goals and building resilience to climate impacts across Europe.

2.2. Carbon cycling in wetland ecosystems

2.2.1. Current status of carbon cycling in wetland ecosystems

Wetlands are among the most productive ecosystems, playing a crucial role in regulating the global carbon cycle. R_{eco} (ecosystem respiration) is the largest component of carbon export from terrestrial ecosystems and determines their carbon sequestration potential. R_{eco} in wetlands is influenced by several environmental factors, meteorological parameters, as well as physicochemical parameters of water and soil.

CO_2 emissions from the water-atmosphere interface depend on T_{water} (water temperature)[13], T_{air} (air temperature) [14], vegetation type, root biomass [15], and hydrological conditions [34]. The rate of CO_2 exchange between soil and air is directly influenced by soil and air temperature, M_{soil} (soil moisture), soil properties [16], salinity [17], and nutrients.

2.2.2. Riparian wetlands in the global carbon cycle

Riparian wetlands have the capacity to sequester soil carbon while managing CH_4 emissions, making them key ecosystems; thus, regulatory frameworks recognize their dual role in sequestering carbon and regulating GHG emissions, directly linking to the role of riparian wetlands in the global carbon cycle.

C captured in wetlands is primarily stored as OM in flooded soils, where anaerobic conditions slow decomposition, leading to carbon accumulation over time [18]. CO_2 and CH_4 emissions from water reservoirs/wetlands result from the decomposition of OM from plants, flooded soils/mud, the decomposition of OM produced in the reservoir, and OM imported into it through flooding. CO_2 is produced under oxic (in the presence of oxygen) and anoxic (in the absence of oxygen) conditions in the water body, in the flooded soils and sediments of the reservoir/wetland, and is consumed by aquatic primary producers (living biomass, microorganisms) [19].

During flood periods, OM and C-rich sediments are deposited in wetlands, where they can be stored in anaerobic soil layers, reducing decomposition rates and promoting long-term C storage [20]. In conclusion, riparian wetlands can accumulate large stocks of C_{org}, especially in the soil, where C can remain stored for a long time [18].

2.3. The main parameters influencing CO_2 emissions from wetland ecosystems

2.3.1. Dependence of CO_2 emissions on meteorological parameters

Recent research in the field has identified T_{air} [21][22], Pp (precipitation) [23], P* (atmospheric pressure) [21], and solar radiation [24] as key meteorological factors influencing CO_2 emissions from wetlands. Determining the dependency relationships between meteorological conditions and CO_2 emissions from wetlands is essential for developing accurate GHG inventories and for modeling the impact of climate change on wetland carbon dynamics.

T_{air} is the main meteorological factor influencing soil microbial respiration, leading to increased decomposition of C_{org} stored in wetland soils and subsequent release of CO_2. Higher temperatures enhance R_{plant} (plant respiration) [25], as part of the natural metabolic processes of vegetation, leading to greater CO_2 release [26].

Precipitation has a significant impact on CO_2 emissions from wetlands, influencing water levels, oxygen availability, and microbial activity, all of which are key factors in GHG fluxes [27]. Variations in precipitation patterns enhance the loss of C stored in wetland soils.

Atmospheric pressure is an important parameter that influences CO_2 emissions in wetlands by influencing the rates of CO_2 exchange between the soil and the atmosphere, as well as by affecting microbial activity in the wetland ecosystem. Gas exchange and diffusion are influenced by P*, with lower pressure increasing gas release from wetland soils and higher pressure slowing CO_2 emissions [28]. Water levels in wetlands can also be affected by atmospheric pressure, with higher pressure pushing water deeper into the soil and lower pressure creating a suction effect, releasing trapped gases [29].

Wind speed (VV) has a significant impact on CO_2 emissions from wetlands, affecting gas exchange rates and microclimate conditions. Wind increases water turbulence, enhancing the transfer of CO_2 from the water-atmosphere or soil-atmosphere interface. This effect can temporarily increase CO_2 emissions, especially in areas with surface water [30].

2.3.2. Dependence of CO_2 emissions on the physico-chemical parameters of water

T_{water} is the main parameter among all variables that influence the rate of biochemical processes such as photosynthesis, microbial respiration, or OM decomposition. As T_{air} and T_{water} increase, the metabolic activity of aerobic and anaerobic microorganisms intensifies, leading to higher respiration rates and, consequently, to increased CO_2 emissions [31]. $Q10_{water}$ is a function that estimates how much the reaction rate of microorganisms increases with a 10°C increase in water temperature. $Q10_{water}$ values are high for many microbial processes that occur in wetlands, which means that CO_2 emissions can increase significantly even with small increases in temperature [32].

DO (dissolved oxygen) is essential for the respiration of aquatic organisms, and at low levels, it slows down microbial activity, leading to anaerobic processes that generate CO_2 and CH_4 emissions [33]. In these cases, wetlands can shift from being CO_2 sinks to contributing CH_4 emissions to the atmosphere. Also, low DO levels due to OM accumulations or pollution can lead to hypoxic conditions (lack of oxygen) that are stressors for dependent organisms, thus reducing biodiversity and altering ecosystem dynamics [34].

Water *pH* also influences the carbon cycle through microbial activity. The types of microbial processes influence whether the main product of OM decomposition is CO_2 or CH_4.

Nutrients, such as nitrogen (N), phosphorus (P), and potassium (K), influence both plant productivity and microbial decomposition processes, which in turn influence the overall carbon balance and GHG emissions.

Chlorophyll-a is the main pigment in algae and aquatic plants, stimulating primary productivity and influencing CO_2 emissions. This has a dual effect; on the one hand, it can promote the absorption and storage of CO_2 through photosynthetic activity, but, under certain conditions, it can indirectly lead to increased CO_2 emissions through decomposition and microbial processes.

Turbidity and *TSD* (total dissolved salts) are factors that obstruct the access of light in aquatic ecosystems, influencing photosynthetic processes, bacterial activity, and OM decomposition. When turbidity is high, light is more difficult to penetrate, which reduces the efficiency of photosynthesis and favors anaerobic conditions, thus altering the balance between CO_2 and CH_4 emissions [35]. Water with high turbidity often indicates the presence of large

amounts of OM in suspension or sediments, elements that contribute to increased levels of CO_2 emissions [36]. Dissolved salts such as bicarbonates and carbonates have the ability to influence pH, which affects the solubility of CO_2 and implicitly its emissions [37].

2.3.3. Dependence of CO_2 emissions on soil physicochemical parameters

Microbial activity is primarily affected by T_{soil}. Wetland soils contain a large amount of OM, which includes labile and recalcitrant carbon pools. While recalcitrant carbon typically decomposes more slowly, the latter decomposes rapidly and releases CO_2 through microbial respiration [38]. Similarly, increases in T_{soil} release stored C from pools that were otherwise stable.

Soil moisture has a direct impact on the microbial processes that contribute to OM decomposition and CO_2 emissions. The types of microorganisms that control the decomposition process influence the rate of OM decomposition in wetlands, as moisture availability influences soil oxygen levels [39].

Soil pH in wetlands influences enzymatic activity, nutrient availability, and soil redox status. Water chemistry, plant species, microbial populations, and hydrological conditions influence soil pH, determining whether a wetland acts as a sink or source of CO_2 emissions. Since soil nutrients affect microbial populations, plant production, and the decomposition of dead OM, they are essential in determining CO_2 emissions from aquatic ecosystems. During OM decomposition, microbial growth and enzyme performance depend on N and P [40]. Wetland ecosystems can suffer from nutrient overload, which can cause eutrophication and convert wetlands from carbon sinks to sources [41].

2.4. Methods for determining CO_2 fluxes from aquatic and terrestrial ecosystems

For monitoring CO_2 fluxes at the soil-atmosphere and water-atmosphere interfaces, established techniques and methods include direct measurement approaches using in-situ sensors and GHG chambers, and advanced satellite monitoring and biogeochemical modeling techniques. Each method offers advantages and limitations, based on which a decision analysis was performed to evaluate the models and their satisfaction, presented in Figure 2.1.

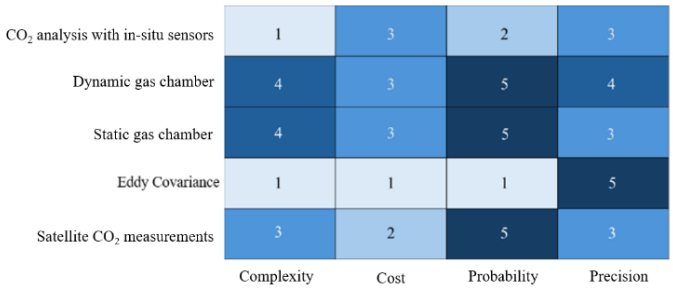


Fig. 2.1. Decision matrix for choosing methods for determining CO_2 fluxes

From the analysis of the decision matrix, it results that the highest satisfaction coefficient is for the dynamic camera (80%), respectively the static camera (75%).

2.5. Methods for estimating CO_2 emissions

Data analysis for the purpose of estimating CO_2 emissions at a spatiotemporal level involves hybrid approaches that combine quantitative and qualitative methods that include scenarios based on numerical methods that include extrapolations of some parameters, as well as specific numerical and biogeochemical models. Different scenarios with emission trajectories and greenhouse gas concentrations according to the RCP (Representative Concentration Pathways) are frequently used for modeling CO_2 emissions. Numerical modeling in space and time is used to calibrate and validate the obtained results, which is achieved through the temporal dynamics of in-situ measurements.

Extrapolations are methods for studying CO_2 fluxes on a large scale, providing an overview of carbon dynamics, and to obtain data with a high level of confidence, they combine direct measurements and predictive models. Extrapolations require validation and calibration based on in-situ monitoring measurements made in the past for a type of ecosystem, after which they proceed to extrapolation into the future.

To analyze the processes that control the carbon cycle at the ecosystem level, biogeochemical models are most often used to integrate biological, chemical and physical factors. One of these tools is the DNDC (DeNitrification-DeComposition) model, which is a biogeochemical tool that allows the simulation of GHG fluxes from both terrestrial and aquatic ecosystems. It is important to note that DNDC requires a detailed set of initial parameters, and possible errors can occur in the absence of detailed or erroneous input data, or with a low level of confidence.

Another method for estimating CO_2 emissions at the global level is the integration of satellite data or data obtained through remote sensing using drones. Satellite remote sensing provides an efficient method for monitoring CO_2 emissions, measuring gas concentrations through infrared spectroscopy, on the other hand, drone remote sensing provides estimates of local gas fluxes and ensures high spatial resolution and accessibility in more isolated areas [42].

CHAPTER 3. MATERIALS AND METHODS

3.1. Characterization of the study area

The researched area represents a segment of the Dâmbovița River, where it forms small wetland ecosystems, with notable biodiversity, due to local habitat conditions and proximity to the city. In the area upstream of Morii Lake, the river retains some of its natural characteristics, although it has been largely subjected to hydrotechnical developments.

These natural wetlands have an essential ecological role, forming aquatic habitats, contributing to water retention, bank stabilization and, in some cases, to the filtration of pollutants before reaching Morii Lake [43]. However, the proximity to Bucharest and the accelerated urban development in the vicinity of Chiajna commune exert significant pressure on these habitats.

3.2. Spatial distribution of the Dâmbovița River study area

The terrain in this region is generally flat with slight elevations, typical of the Romanian Plain. Slight unevenness of the terrain can affect the flow of surface water and influence the potential flood risks in low-lying areas.

Taking into account the geographical coordinates, as well as a series of databases, maps were processed in the QGIS (Quantum Geographic Information System) program, highlighting the types of land cover for the years 1984 to 2020 as well as the determined area within the study area.

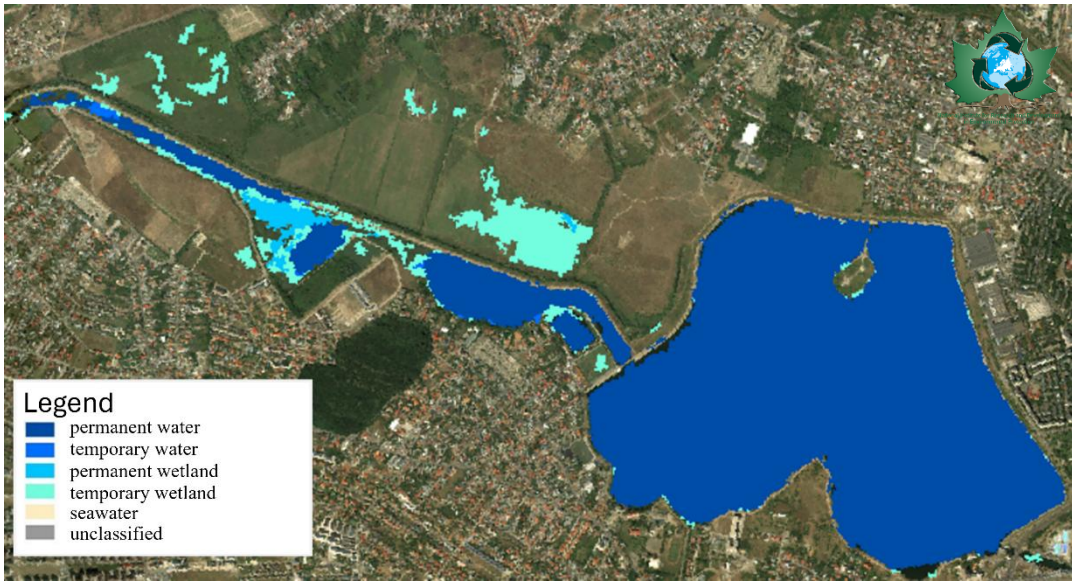


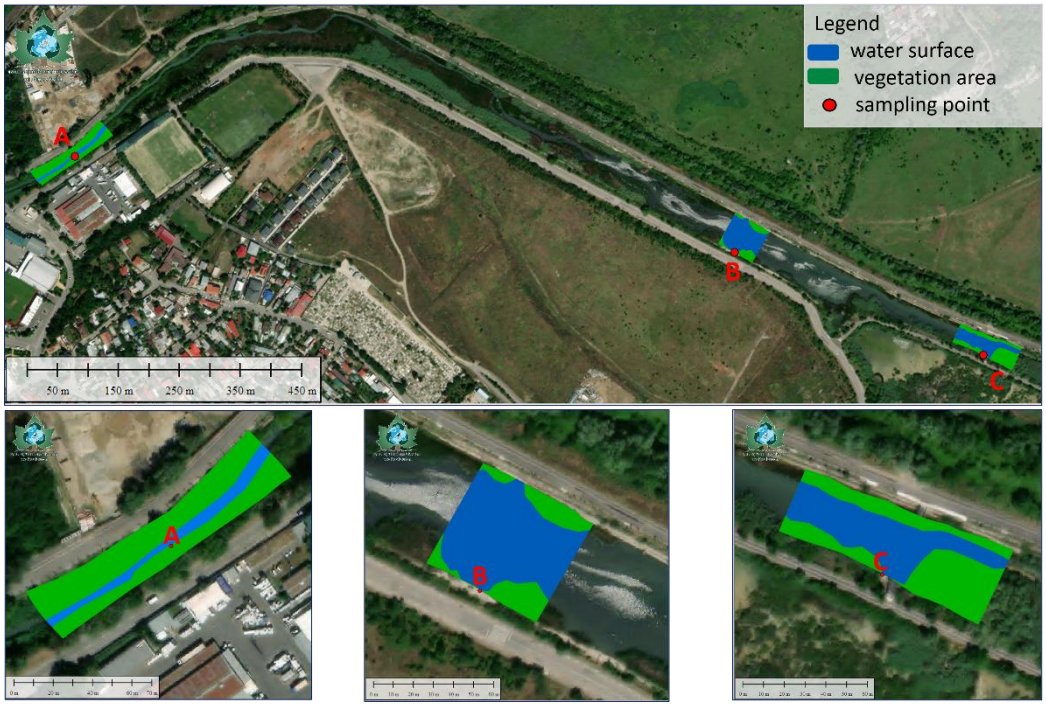
Fig. 3.1. Determination of wetland areas in the study area using the Corine Land Cover methodology

3.2.1. Spatial situation of the water body in the investigated area (Dâmbovița River area)

Since the construction of the Lacul Morii reservoir in 1986, fluvial wetlands have formed upstream of it, covered by specific vegetation of the species *Phragmites australis* and *Typha latifolia*. The area considered in the case study, shown in Figure 3.2, has a perimeter of 8630 m and a surface area of 702,604 m^2. In order to capture the variability of the entire study area, the three most suggestive areas of equal area along the river for measurements of CO_2 emissions at the water-atmosphere interface (Area A, Area B and Area C) were selected based on the spatial distribution and extent of vegetation. Thus, Area A corresponding to Location A, located upstream, is characterized by a narrow river course on a naturally developed riverbed, having a higher flow speed compared to the other analyzed locations, and its banks are abundantly covered with *Typha latifolia* vegetation. In the summer season, vegetation presents 61.65% of the total area of 3606 m^2, while the water surface has an area of 38.35%. Area B, corresponding to Location B, has a wider bank than Area A, a built riverbed and mixed vegetation dispersed along the banks. This is considered a transitional area between Area A and C in terms of vegetation distribution. In summer, vegetation presents 37.44% of the total area of 3600 m^2, while the water surface has an area percentage of 62.56%. Area C, which corresponds to Location C, was selected for its positioning as close as possible to the constructed reservoir, but also for the soils abundantly covered by *Phragmites australis* vegetation in a proportion of 37.44%, while the water surface presents a percentage of 40.85% of the total area of 3655 m^2.

It is known that CO_2 emissions depend on the area of the vegetation area, respectively, on the geometric shape of the analyzed wetland. In this context, a shape coefficient of the wetland geometry CND= f (vegetation area /water area, width/length of investigated area) was

identified that characterizes CO_2 emissions. For each area investigated, this adjustment coefficient was calculated with the values: Area A=0.25, Area B=0.43, Area C=0.54.



C_{ND}=0.25 C_{ND}=0.43 C_{ND}=0.54

Fig. 3.2. Spatial representation of CO_2 emission measurement areas at the water-atmosphere interface

3.2.2. Spatial situation of the soil in the investigated area (Dâmbovița River area)

The study areas for the measurements of CO_2 fluxes from the soil surface, represented in Figure 3.3, were selected according to the type of vegetation covering it and the humidity regime. Thus, in the study area, two types of soil were identified: potentially floodable soil and flooded soil, but also two types of vegetation specific to wetlands: bulrush (*Typha latifolia*) and reed (*Phragmites australis*). The soil area with predominant vegetation of the rush species is located in the immediate vicinity of the Dâmbovița River, in the upstream area (Location SC). From a management point of view, this is a soil with flood potential, but throughout the measurement period, it was not covered by the river waters. The second soil type selected for monitoring is located in the downstream area and is characterized by vegetation predominantly of the reed species (Location SP). It had a discrepant humidity regime throughout the year; thus, in the first part of the year, during January-May, it presented the characteristics of a dried soil, with humidity values between 11.6% and 45.6%, and during June-December, it was saturated with water, with humidity values of over 50%.



Fig. 3.3. Spatial representation of CO_2 emission measurement areas at the soil-atmosphere interface

To determine the degree of litter degradability, two types of vegetation, *Phragmites australis* and *Typha latifolia*, were collected in the fall, given that these are the most common aquatic plant species along the Dâmbovița watershed in the study area upstream of Lake Morii. To approximate natural conditions, the vegetation was cut in the drying phase, in order to capture the entire process of its degradation. To minimize differences in litter quality, each species was collected from the same area (Area A), shown in Figure 3.4.



Fig. 3.4. Spatial representation of the surface biomass collection area for the species *Phragmites australis* and *Typha latifolia*

3.3. Climate and climate change signal analysis

3.3.1. Climate and climate variability analysis of the investigated wetland

In order to analyse the main meteorological parameters, reanalysis data generated by ECMWF (European Centre for Medium-Range Weather Forecasts) through ERA5 (ECMWF Reanalysis v5) at a spatial resolution of 30 km for the time interval 1979-2023 were used (Figure 3.5) [44][45].

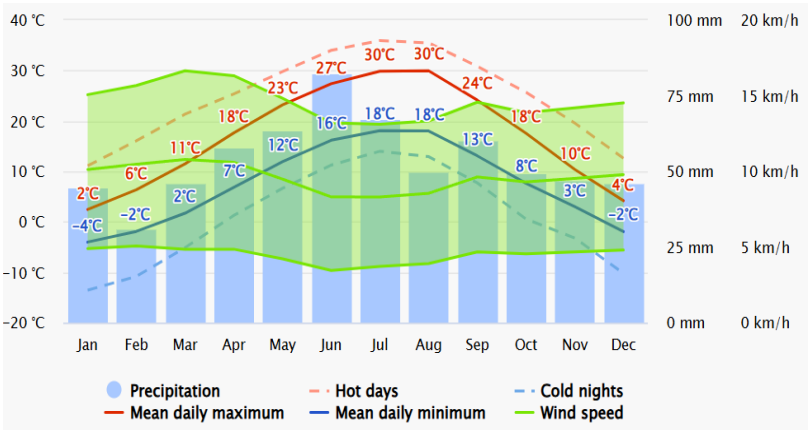


Fig. 3.5. Average temperature, average precipitation and wind speed over the last 30 years [155]

The graph in Figure 3.6 shows the temperature and precipitation anomaly for each month from 1979 to the present. In terms of temperatures, there is an increase in warmer months over the years with anomalies of up to 5.6 °C in January 2023 reflecting global warming associated with climate change. Also, the highest negative values of temperature anomalies were recorded in February 1985 and 2012 with -9°C and -7.3°C, respectively, compared to the monthly average. Months with precipitation anomalies were recorded in September 2005 with 177 mm and in July 1991 with 132 mm. Negative values indicating dry months have been predominant in the last 20 years, with anomaly indicators of up to -63 mm in July 2012.

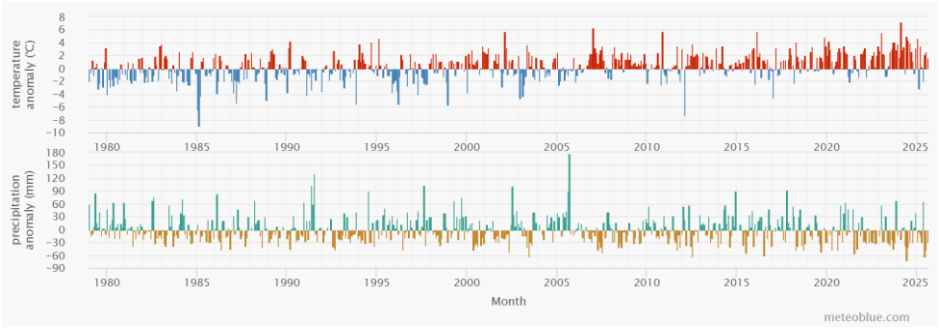


Fig. 3.6. Monthly temperature and precipitation anomalies in the period 1979-2023 [44]

3.3.2. Climate change projection for the investigated wetland

Climate model data available from the Climate Analytics platform [45] were used for this analysis.

The graph in Figure 3.7 shows how the absolute changes in average air temperature will unfold over time in the Bucharest region at different levels of global warming based on the RCP 8.5 and RCP 4.5 scenarios. These are compared with the reference period between 1986 and 2006, when the average temperature was 11.69 °C. Thus, according to RCP 4.5, by 2050, an increase of 1.9°C was simulated, and according to RCP 8.5, the increase is 2.3°C. By 2100, daily minimum values may increase by 3.1°C according to RCP 4.5 and by up to 6.6°C, above the average of the base years, according to RCP 8.5.

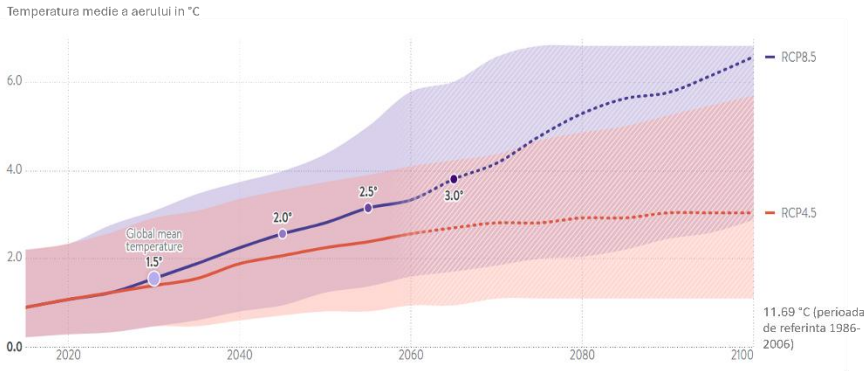


Fig. 3.7. Average air temperature modeled according to RCP 4.5 and RCP 8.5 [45]

3.4. Methodology for monitoring CO_2 emissions

3.4.1. Monitoring CO_2 emissions from the soil-atmosphere interface

The method used to measure emissions at the soil-atmosphere interface is based on the direct measurement of CO_2 fluxes inside a chamber with a known surface area [159]. To measure soil respiration, within the INCDPM, a portable infrared CO_2 gas analyzer (EGM-5) (Figure 3.8) was used, equipped with a sensor (Stevens HydraProbe) for soil temperature and moisture analysis. The method is dynamic and is based on measuring the difference in CO_2 concentration (ppm) between the air entering and leaving the chamber. CO_2 emissions were determined by measuring the rate of change (increase) of the rate of CO_2 concentration inside the chamber over a predetermined period [46].



Fig. 3.8 Closed dynamic chamber CO_2 flux analyser EGM-5

Monitoring was based on the repeatability of a measurement between three and five repetitions lasting 60 seconds each. The emission rate at each point was then estimated using the arithmetic mean method [47]. The methodology for measuring CO_2 fluxes in each area was carried out monthly, with repetitions in months in which meteorological anomalies were identified, such as precipitation after a long period of drought or abnormal temperatures for the targeted period.

3.4.2. Monitoring CO_2 emissions from the water-atmosphere interface
3.4.3. Dynamic closed chamber method

To perform CO_2 flow measurements at the water-atmosphere interface, the equipment consisting of the EGM-5 analyzer and the closed dynamic chamber was adapted to the specific conditions of aquatic ecosystems and was placed on a floating device designed by the author within the INCDPM (Figure 3.9).



Fig. 3.9. EGM-5 closed chamber system and floating device

Because the measurement time directly depends on the linear respiration of the ecosystem, and to adapt the closed-chamber measurement methodology of CO_2 flow in wetlands, the measurement time was increased to 300 sec, the maximum allowed by the capacity of the device [48].

3.4.4. Injection Kit Method

An alternative to the closed dynamic chamber method is the Injection Kit method, a technique used to measure CO_2 concentrations using small gas samples collected in a static sampling chamber and transferred to the EGM-5 analyzer using a syringe.

The Injection Kit (Figure 3.10) consists of two main components: a network of tubes that connect to the static chamber, the static chamber in which the CO_2 accumulates, and a series of 10 ml injections for collecting gas samples that allow monitoring the CO_2 concentration inside the static chamber. For the collection of CO_2 from the water-atmosphere interface, within the INCDPM, a floating static collection chamber with a known Vc (volume) of 4.25 l was used.



a) b) c)

Fig. 3.10. Injection Kit for collection (a) and analysis (b) of CO_2 from the water-atmosphere interface and collection method from the soil-atmosphere interface (c)

The principle of the EGM-5 closed chamber CO_2 flow measurement method is based on the difference between the atmospheric CO_2 concentration and the CO_2 emissions from the surface, calculated automatically by the device. On the other hand, the Injection Kit method measures the CO_2 concentrations accumulated inside the chamber placed on the water surface over a period of 30 minutes. Samples were collected systematically every 1 minute for the first 5 minutes, every 3 minutes for the next 15 minutes, then 2 measurements every 5 minutes [48].

3.6. Monitoring of physico-chemical parameters of water

3.6.3. Water sampling and laboratory analysis

In order to determine the water and soil quality parameters for a comparative analysis, water and soil samples were taken in May from each study area in order to ensure a high level of confidence in the monitored parameters.

For water sampling, a quantity of 500 ml was collected for each sample at a depth of approximately 30 cm. The container was inserted with the opening down in the water for deep sampling, then the bottle was held against the current until it was filled. The containers were labeled and transported to the INCDPM laboratory, kept cool and away from sunlight. The sample analysis focused on pH parameters, the main nutrients such as N and P, CCO-Cr, and *Chlorophyll-a.*

3.6. Monitoring of soil physicochemical parameters

3.6.2. Soil sampling and laboratory analysis

In order to determine the water and soil quality parameters, water and soil samples were taken in May, from each study area. According to the methodology, for each sample area, near its center, a soil profile was made, which was dug using a shovel, and soil samples were taken with a metal cylinder with dimensions of 25 cm in length and 5 cm in diameter [49]. Two samples for each soil profile were collected from depths of 0-10 cm, 25-30 cm, the amount of soil taken for each geometric horizon being between 87 g and 124 g. The bags with the soil samples from the field were labeled (date number and geometric horizon), and sent to the INCDPM laboratory for determinations of pH, total nitrogen (N_{total}), total phosphorus P_{total}, $C_{org,}$ and humus. All samples were dried for 48h at a temperature of 40°C, to a constant mass [50], and roots and stones were removed.

3.7. Analysis of the composition and dynamics of litter degradability

3.7.2. Monitoring the rate of litter degradability

The litter bag method is the predominant method reported for estimating litter decomposition rates in both terrestrial and wetland environments [184]. This method involves placing a known amount of litter in a fabric bag or mesh and then examining the temporal pattern of weight loss with a series of collections over a period of several weeks to several years.

We measured litter decomposition through activities undertaken within the INCDPM, using the litter bag method [51]. In November 2022, we collected two types of vegetation: reed (*Phragmites australis*) and bulrush (*Typha latifolia*), as they are the main common plant species dominant for the study wetland. To approximate natural conditions, the vegetation was cut in the drying phase, but while still standing, to capture the full process of its degradability. To minimize differences in litter quality, each species was collected from a single area, from Location A.

The litter bags were hand-made from 150x150 mm fiberglass mesh, with one folded side and three sides sewn with thread of the same material [52]. Each bag was labeled with a unique identification code to allow the final weights to be matched to the initial weights [53]. Each bag was weighed with a precision balance before filling to avoid weight errors that could have occurred from their manual construction. Thus, 40 bags were filled, 20 with each type of vegetation between the two; thus, the amount of 10g of litter was the same in each bag. Subsequently, the bags were grouped by 5 with content from each vegetation species and tightly tied along a string with a total length of approximately 2m each. The bags were first submerged to minimize any hydrophobic effect that the mesh they were made of might have caused.

Four replicates of each vegetation type were sampled on the day of placement to calculate mass loss due to handling [54]. Eight series of 5 bags were then extracted 10 days apart. The litter bags were transported back to the INCDPM laboratory, cleaned of external material, and opened. Debris was carefully removed from inside the bag, and sediment was rinsed. The litter was oven-dried at a constant temperature of 65 °C for approximately five days until a constant mass was reached [55], the mass was recorded, and the litter was then ground to a powder.



Fig. 3.11. Cleaning and drying stages of the litter

3.7.3. Estimating the carbon content of litter

Field collection of samples from the litter horizon was carried out according to the methodology in the specialized literature, at a distance of 1m between each sample area.

The litter consisted of willow leaves (*Salix Sepulclris Chrysocoma*) and wood residues originating from it in total proportion. It was considered necessary that, for each sample area, five samples from the litter horizon be collected, from inside a square wooden frame with a side of 20 cm. At the same time, mineral residues and stones were removed, as OM was collected from inside the frame. The litter samples consisting of dry leaves and wood residues (those with a diameter of less than 1 cm) were placed individually from the field in labeled plastic bags.

To convert green mass into dry mass, litter samples were dried in the INCDPM laboratory, in an oven, at a temperature of 65°C for a period of 72 hours [194]. Separate weighing of components (leaves and wood) was performed with a high precision balance (+ 0.01 g). C_{org} quantification was obtained using the expeditious method proposed by several authors [195][196] by multiplying the amount of dry OM by the conversion factor 0.5. The result obtained was expressed in t/ha.

3.8. Data analysis

Carbon dioxide emissions are influenced by multiple factors directly or indirectly. For the entire factor analysis process, a statistical analysis software called SPSS 29.0 (Statistical Product and Service Solutions) [56] was used.

For data analysis and graphical representation of the results, we used the Origin Pro 2024 software, provided by OriginLab [57].

In the study, the DNDC software [58] was used to generate scenarios of greenhouse gas emissions and fluxes for the years 2050 and 2100. DNDC was chosen due to its ability to model complex biogeochemical processes, including interactions between soil, vegetation, and atmosphere. The software was also calibrated using field data, thus ensuring a realistic and accurate representation of the dynamics of the studied ecosystems.

CHAPTER 4. RESULTS AND DISCUSSIONS

4.1. Physico-chemical characterization

4.1.1. Physico-chemical characterization of water

To characterize the water quality of each research location, laboratory analyses of the main indicators were performed within the INCDPM. The results of the water samples collected from the three locations (Location A, Location B, Location C) established along the river course are presented in Table 4.1.

Table 4.1. Physico-chemical water quality indicators characteristic of each study location

Indicator		Location A	Location B	Location C
pH	**pH (t°C)**	7.54 (21.4)	7.36 (21.8)	7.39 (22.1)
N_{total}	**mg N/l**	3.92	4.20	8.40
P_{total}	**mg P/l**	0.123	0.243	0.333
CCO-Cr	**mg O_2/l**	5.98	15.3	9.4
Chlorophyll-a	**µg/l**	1.18	4.74	3.55

To characterize the three investigation areas A, B and C from the point of view of water quality, a decision matrix was created, in which, for good conditions, a maximum qualitative value of 3 was considered, moderate 2, and poor 1, presented in Table 4.2.

Table 4.2. Decision matrix for the physicochemical characterization of water

	Location A	Location B	Location C
pH	Alkaline	Alkaline	Alkaline
N_{total}	3	2	1
P_{total}	3	2	1
CCO-Cr	1	3	2
Chlorophyll-a	1	3	2

Based on the decision matrix, it results that, from the pH values in the 3 locations, it indicates a moderate alkalinity. From the point of view of N_{total} and P_{total}, the decrease from upstream to downstream of the concentrations is observed. For chlorophyll-a, respectively, the parameter related to dissolved oxygen and CCO-Cr, it is observed that in Location A we have the lowest values, in Location B the highest, respectively in Location C, moderate values. Following the processing of the qualitative data presented in Table 4.2, it results that in Location A, the water body is characterized at 66% very good from the point of view of the ecosystem, in Location B with 83% and respectively 50% for Location C.

4.1.2. Physico-chemical characterization of soil

To characterize the soils at each location, soil samples were collected after identifying two vegetation types and distinct moisture regimes of the soil. Table 4.3 presents the results for soil quality indicators at depths of 15 cm and 30 cm.

Table 4.3. Physico-chemical characteristics of soil depending on depth and location

		SC		SP	
Indicator	**U.M.**	**15 cm**	**30 cm**	**15 cm**	**30 cm**
pH/T_{air}	**pH/(°C)**	7.06/23.3	7.42/23.3	6.21/23.3	7.49/23.3
N_{total}	**%**	0.433	0.488	0.074	0.008
P_{total}	**%**	0.083	0.058	0.072	0.082
C_{org}	**%**	2.13	2.74	1.95	6.38
Humus	**%**	3.67	4.73	3.37	11

4.2. Dynamics of CO_2 fluxes from the reservoir - validation of the IPCC Guidance hypothesis

Potential CO_2 emissions from the water-atmosphere interface in Morii Lake were monitored during the summer period, when its respiration should be maximum. Weekly measurements were carried out during the period July-September, and the measured emission values were predominantly negative (Figure 4.1). The minimum obtained was recorded in July of -0.07404 g $m^{-2}h^{-1}$, and the maximum was in August of 0.01489 g $m^{-2}h^{-1}$. Through these series of values, it is considered that the existence of equilibrium conditions has been verified, which means that CO_2 emissions are close to zero and are not taken into account.

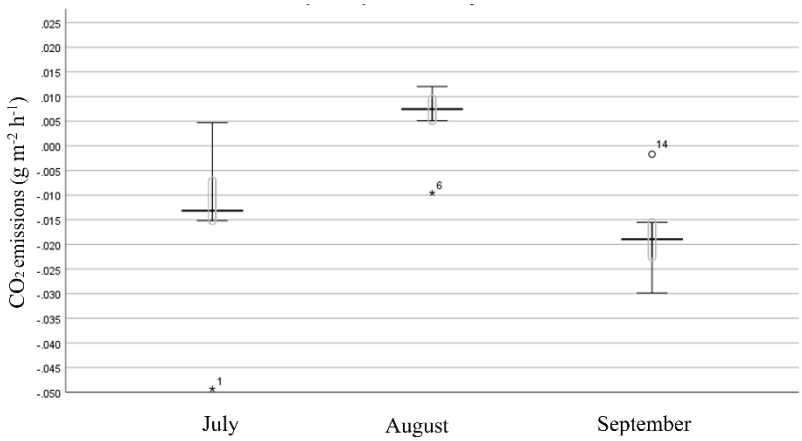


Fig. 4.1. Dynamics of CO_2 emissions from Morii Lake

Considering that, according to the IPCC Guidelines, artificial reservoirs emit CO_2 only in the first 25 years after construction, and Morii Lake was completed in 1985–1986, it follows that it exceeded the mentioned emissions period, thus confirming the IPCC statements [1].

4.3. Comparative analysis and optimization of methods for measuring CO_2 emissions from the water-atmosphere interface

This thesis presents two methods for measuring CO_2 emissions, described in Chapter 3 and performs a comparative analysis of them in order to improve the information volume that can be the basis for decisions with a high level of confidence in terms of contributing to the inventory of GHG emissions of wetlands. The measurements obtained by the EGM-5 methods and the Injection Kit during the year 2022 allow the analysis of temporal variations in CO_2 emissions from the water-atmosphere interface in the study area and are presented in Figure 4.2, through cumulative values on Locations A, B, and C for each month of the study year.

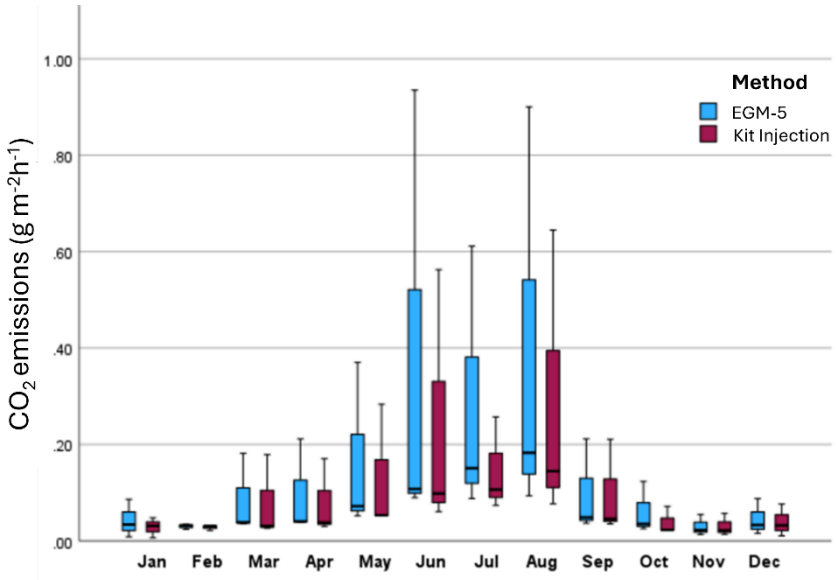


Fig.4.2. Monthly variation of CO_2 emissions measured cumulatively at the 3 locations with the EGM-5 method and the Injection Kit method

To evaluate the results obtained by the two methods, the statistical analysis of the Pearson correlation coefficient was used to identify whether there is a dependence between the two methods of measuring CO_2 emissions for each month, the results being presented in Table

4.4. The results obtained on the monthly average values from the 3 locations show that the Pearson correlation coefficient presents a strong positive statistical significance [59] in each month ($p<0.01$ and $p<0.05$), ranging between 0.912 and 0.999. Thus, it was shown that both methods measure CO_2 emissions well in the area of interest, the distributions having similar monthly trends, but with different amplitudes in favor of the EGM-5 method. This aspect shows that the two methods are complementary at the general level of the study area throughout the year and characterize CO_2 emissions in periurban wetlands.

4.3.1. Comparative analysis of methods for measuring CO_2 emissions from the water-atmosphere interface

The variations in average CO_2 emissions measured using the EGM-5 and Injection Kit methods in each of the 3 study locations (Location A, Location B, and Location C) are analyzed below. Figure 4.3. shows the variation in average monthly CO_2 emissions in Location A.

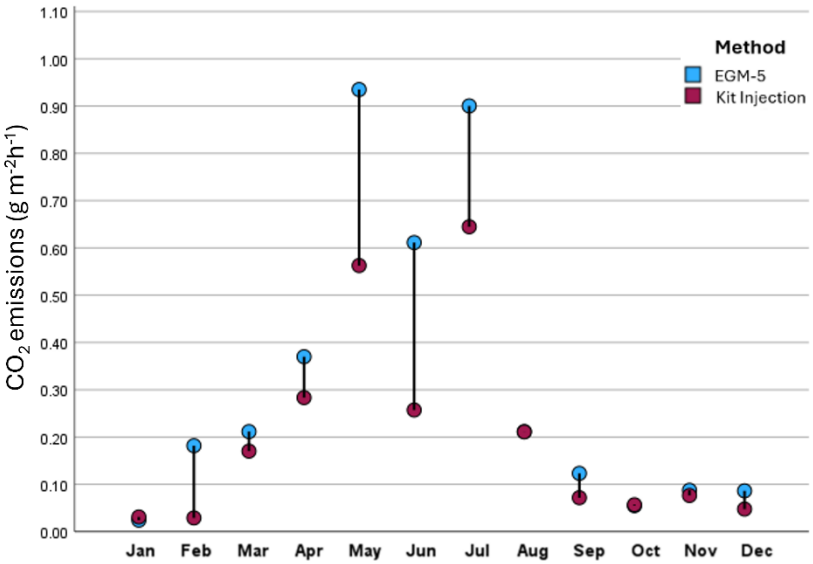


Fig. 4.3. Monthly variation of average CO_2 emissions from Location A measured with the EGM-5 method and the Injection Kit method

The results of the t-test ($t=1.019$, $p=0.122$) indicated a statistically insignificant difference between the two measurement methods for the monthly averages of CO_2 emissions at the annual level in Location A, respectively, the ANOVA analysis ($F=1.038$, $p=0.319$). For Location A, the values of the annual average CO_2 emissions measured by the EGM-5 method and the Injection Kit method show that the difference is insignificant.

In Figure 4.4. the variation of the monthly average CO_2 emissions in Location B is represented.

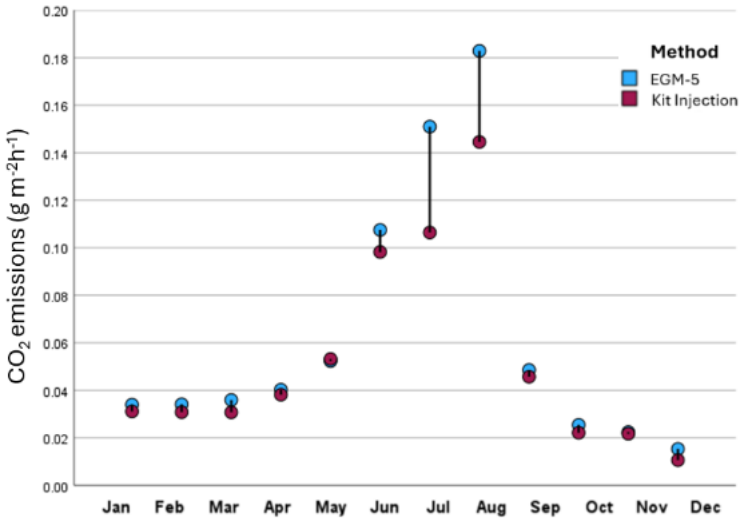


Fig. 4.4. Monthly variation of average CO_2 emissions from Location B measured with the EGM-5 method and the Injection Kit method

The results of the t-test (t=0.009, p=0.492) indicated a statistically insignificant difference between the two measurement methods for the annual averages of CO_2 emissions in Location B, respectively, the ANOVA analysis (F=0.242, p=0.628). For Location B, the values of the annual average CO_2 emissions measured by the EGM-5 method and the Injection Kit method show that the difference is insignificant.

Figure 4.5. shows the variation in average monthly CO_2 emissions in Location C.

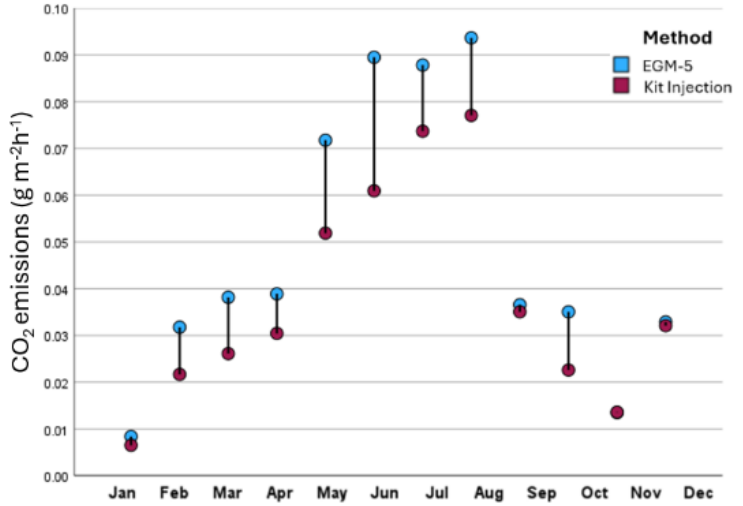


Fig. 4.5. Monthly variation of average CO_2 emissions from Location C measured with the EGM-5 method and the Injection Kit method

The results of the t-test (t=0.970, p=0.260) indicated a statistically insignificant difference between the two measurement methods for the annual averages of CO_2 emissions in Location C, respectively, the ANOVA analysis (F=0.941, p=0.941). For Location C, the values of the annual average CO_2 emissions measured by the EGM-5 method and the Injection Kit method show that the difference is insignificant.

Table 4.4 presents the results of the t-test and ANOVA for the annual average differences of CO_2 emissions between the EGM-5 method and the Injection Kit method in the three locations.

Table 4.4. Results of t-test and ANOVA for the mean annual differences in CO_2 emissions between the EGM-5 method and the Injection Kit method in locations A, B and C

Location	Method	t-test			ANOVA	
		Annual average difference (g m-2h-1)	t	p (Sig.)	F	p (Sig.)
A	EGM-5	0.112	1.019	0.122	1.038	0.319
	Injection Kit					
B	EGM-5	0.009	0.492	0.377	0.242	0.628
	Injection Kit					
C	EGM-5	0.0105	0.970	0.260	0.941	0.343
	Injection Kit					

The variation of the monthly averages of CO_2 emissions measured with the EGM-5 and Injection Kit methods at the three locations at the water-atmosphere interface (Location A, Location B, and Location C) throughout the year is presented in Figure 4.6. Location A shows a significantly higher annual variation of the measured values, which indicates a high variability. In contrast, for Locations B and C, the variations of the annual averages between the two measurement methods are much smaller.

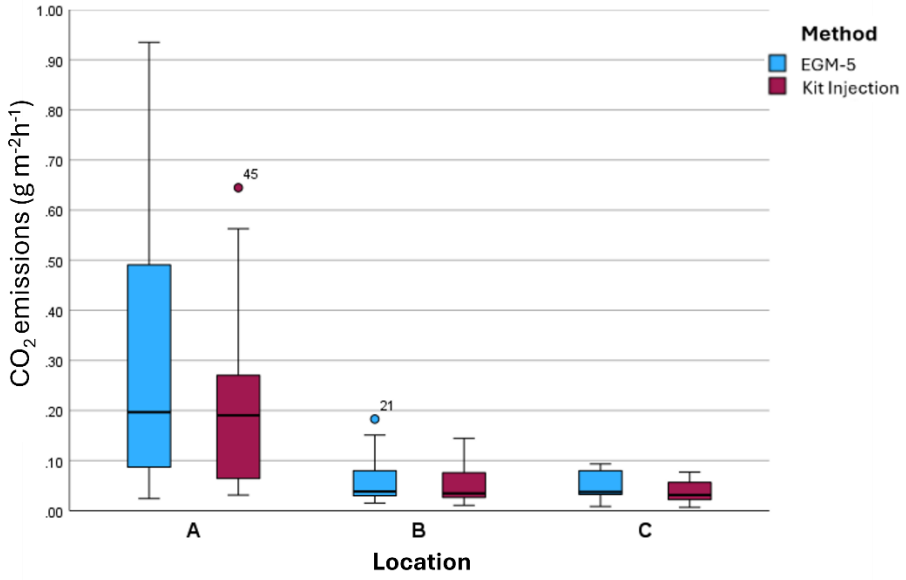


Fig. 4.6. Variation of monthly averages of CO_2 emissions measured with the EGM-5 method and the Injection Kit method at the location level

Statistical analysis of the correlations between the two methods of measuring CO_2 emissions (Table 4.5) on the investigated locations revealed a strongly positive and significant relationship [59] with Pearson correlation coefficient values: Location A ($r=0.956$; $p<0.01$), Location B ($r=0.988$; $p<0.01$), Location C ($r=0.976$; $p<0.01$). This shows that there is an interdependence between the locations in terms of CO_2 emissions.

Table 4.5. Pearson correlation coefficient between the EGM-5 method and the Injection Kit method in Locations A, B, and C

			Location A		Location B		Location C	
			EGM-5	Injection Kit	EGM-5	Injection Kit	EGM-5	Injection Kit
Location A	EGM-5	Pearson correlation	1					
		Sig. (1-tailed)						
	Injection Kit	Pearson correlation	**0.956***	1				
		Sig. (1-tailed)	<0.01					
Location B	EGM-5	Pearson correlation	**0.900***	**0.841***	1			
		Sig. (1-tailed)	<0.01	<0.01				
	Injection Kit	Pearson correlation	**0.939***	**0.903***	**0.988***	1		
		Sig. (1-tailed)	<0.01	<0.01	<0.01			
Location C	EGM-5	Pearson correlation	**0.925***	**0.866***	**0.868***	**0.889***	1	
		Sig. (1-tailed)	<0.01	<0.01	<0.01	<0.01		
	Injection Kit	Pearson correlation	**0.898***	**0.853***	**0.902***	**0.903***	**0.976***	1
		Sig. (1-tailed)	<0.01	<0.01	<0.01	<0.01	<0.01	

*. The correlation is significant at the level 0.01 (1-tailed).

There is an interdependence between the measurement methods used to determine CO_2 emissions in the investigated locations, so that statistical-mathematical models can be developed for periurban wetlands. The statistical-mathematical models regarding the correlation between the two methods of measuring CO_2 emissions between monthly averages are centralized and presented in Table 4.6 and show a very strong correlation [59] in all three analyzed locations, r (0.955÷0.991), respectively, with S (0.0052÷0.997).

Table 4.6. Statistical-mathematical models regarding the correlation between the EGM-5 and Injection Kit measurement methods in the three locations

Location	Independent variable	S	r	Regression equation
A	EGM-5	0.0643	0.955	$a=0.601b+0.0335b^2$
	EGM-5	0.0997	0.955	$b=1.634a-0.2153a^2$
B	Injection Kit	0.0057	0.991	$a=0.977b-1.2146b^2$
	EGM-5	0.0085	0.989	$b=1.025a+1.8841a^2$
C	EGM-5	0.0052	0.976	$a=0.784b-0.1200b^2$
	Injection Kit	0.0065	0.979	$b=1.350a-1.2874a^2$
a=EGM-5 method b=Injection Kit method				

4.3.2. Comparative analysis by season of methods for measuring CO_2 emissions from the water-atmosphere interface

The phenomenon of CO_2 emissions is dependent on climate and implicitly on seasons, especially in the context of climate change, which requires a comparative analysis for the investigated year. The distribution of CO_2 emissions according to the two measurement methods is presented below for each location where measurements were made.

Figure 4.7 shows the variation in the distribution of CO_2 emissions from Location A, where the following aspects are observed:

- in summer and autumn there is a greater variability of emissions,
- in winter the values are the lowest and have an insignificant variability.
- spring is an average variability of emissions

The Pearson correlation coefficient analysis between the two methods of measuring CO_2 emissions proved to be strongly positive and statistically significant [59], independent of the season, but for the development of statistical-mathematical models for periurban wetlands depending on the season, other data sets for at least three more years are needed to expand the database and the level of confidence.

In the winter and spring seasons, the t-test (t=0.578, p=0.295) and ANOVA (p=0.594), and, respectively, the t-test (t=0.996, p=0.819) and ANOVA (p=0.992) do not indicate significant differences between the methods. In the summer, the t-test (t=2.094, p=0.771) shows a significant difference, but ANOVA (p=0.104) shows that this is not statistically significant. In the fall, the t-test (t=0.249, p=0.733) and ANOVA analysis (p=0.815) do not reveal significant differences between the methods.

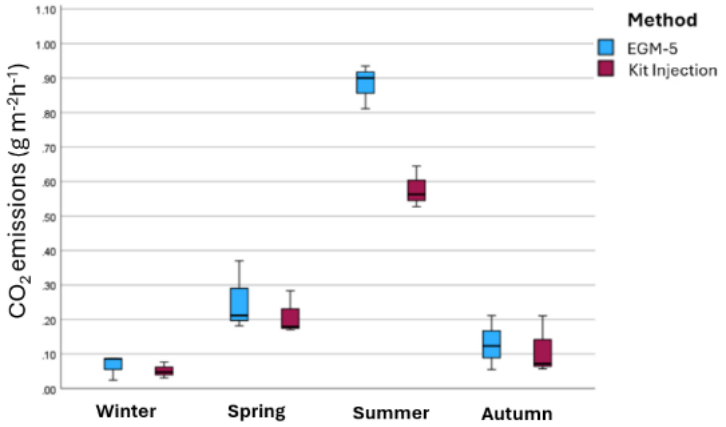


Fig. 4.7. Variation of monthly averages of CO_2 emissions at the seasonal level depending on the method (EGM-5 and Injection Kit) for Location A

Figure 4.8 shows the variation in the distribution of CO_2 emissions from Location B, where the following aspects are observed:

- in summer there is a greater variability of emissions,
- in winter the values are the lowest and have a restricted variability,
- in spring and autumn there is an average variability of emissions.

The analysis of the Pearson correlation coefficient between the two methods of measuring CO_2 emissions, which proved to be strongly positive and statistically significant [59], regardless of the season, but for the development of statistical-mathematical models for periurban wetlands according to the season, other data sets for at least three more years are needed to expand the database and the level of confidence.

In this location, the t-test and ANOVA analysis do not indicate significant differences between the EGM-5 and Kit Injecție methods in any season, so the differences observed are not statistically significant.

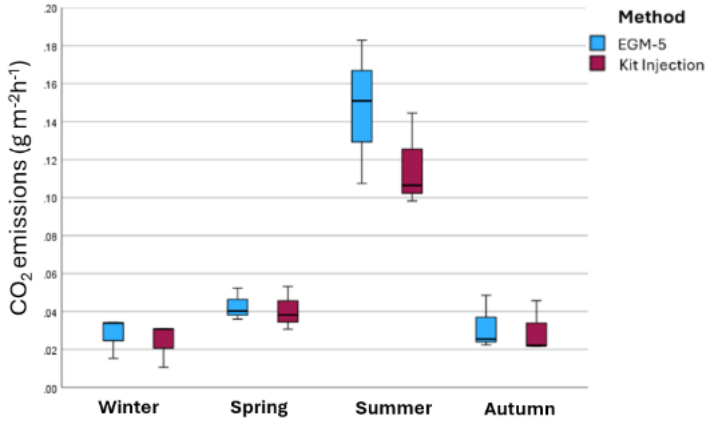


Fig. 4.8. Variation of monthly averages of CO_2 emissions at the seasonal level depending on the method (EGM-5 and Injection Kit) for Location B

Figure 4.9 shows the variation in the distribution of CO_2 emissions from Location C, where the following aspects are observed:

- in summer there is a small variability of emissions,
- in winter and autumn the values are the lowest and have a moderate variability,
- in spring there is an average variability of emissions.

The Pearson correlation coefficient analysis between the two methods of measuring CO_2 emissions proved to be strongly positive and statistically significant [59], independent of the season, but for the development of statistical-mathematical models for periurban wetlands according to the season, other data sets for at least three more years are needed to expand the database and the level of confidence.

In this location, the t-test and ANOVA analysis do not indicate significant differences between the EGM-5 and Injection Kit methods in any season, so the observed differences are not statistically significant.

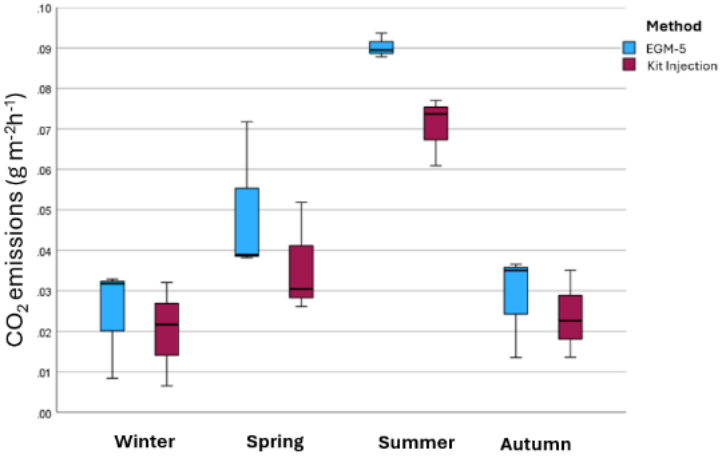


Fig. 4.9. Variation of monthly averages of CO_2 emissions at the seasonal level depending on the method (EGM-5 and Injection Kit) for Location C

4.3.3. Method for improving CO_2 emission measurements in wetlands taking into account their particularities

From the general analysis of the results obtained on the three locations in the investigated area, it results that the CO_2 emissions are dependent on the particularities of the investigated areas. In this context, in order to ensure a high level of confidence regarding the CO_2 emissions on the entire wetland, it was proposed to introduce an adjustment coefficient (C_{ND}) that takes into account these particularities presented in Chapter 3.2. In Figure 4.10, the adjusted values are presented according to the particularities of the geometry and vegetation distribution of the investigated areas.

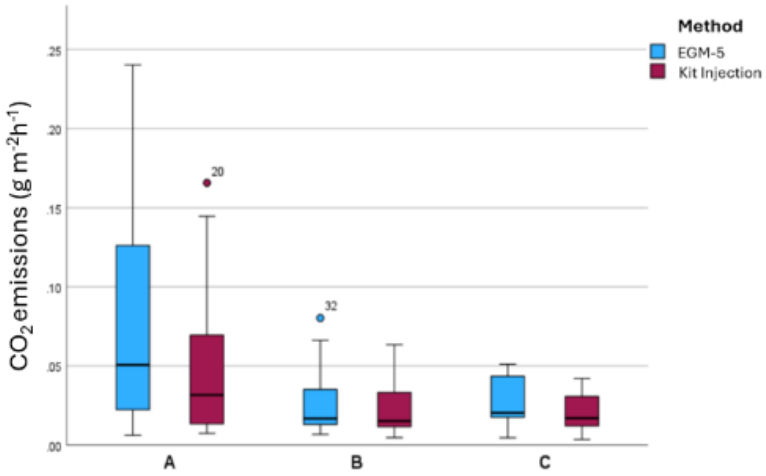


Fig. 4.10 Variation of monthly averages of CO_2 emissions adjusted for the EGM-5 method and the Injection Kit method at the spatial level

From the comparative analysis of the variation of the monthly average of CO_2 emissions measured vs. adjusted with the C_{ND} coefficient, it is observed that the reduction of the amplitude of emission variations and the presentation with a higher degree of confidence of their dynamics over the entire investigated wetland, and the most accurate rendering over the entire area.

The results of the t test (t=2.812, p=0.017 for Area A; t=2.227, p=0.048 for Area B; t=4.182 for Area C) indicated a statistically significant difference between the two measurement methods for the annual averages of CO_2 emissions adjusted by applying the C_{ND} coefficient, but the ANOVA analysis does not confirm the significant differences between the groups (F=1.038; p=0.319 for Area A; F=0.242; p=0.628 for Area B; respectively F=0.942; p=0.342 for Area C).

In this context, statistical-mathematical models were developed that would be generally valid for the entire investigated wetland area. Table 4.7 presents the statistical-mathematical correlations between the EGM-5 and Injection Kit measurements, which are characterized by the fact that, for the three areas, a correlation coefficient r(0.955÷0.991) was obtained as well as the standard error S(0.0025÷0.0256).

Table 4.7. Statistical-mathematical models regarding the correlation between the EGM-5 and Injection Kit methods at a spatial level over the entire investigated area

Area	Independent variable	S	r	Regression equation
A	EGM-5	0.0165	0.955	$a=0.601b+0.1306b^2$
	Injection Kit	0.0256	0.955	$b=1.634a-0.8376a^2$
B	EGM-5	0.0025	0.991	$a=0.977b-2.7669b^2$
	Injection Kit	0.0035	0.989	$b=1.025a+4.2918a^2$
C	EGM-5	0.0028	0.976	$a=0.784b-0.2203b^2$
	Injection Kit	0.0036	0.976	$b=1.350a-2.3633a^2$
a=EGM-5 method b=Injection Kit method				

4.3.4. Seasonal comparative analysis of improved CO_2 emission measurement methods for each area

The seasonal distribution of adjusted CO_2 emissions for Area A measured with the EGM-5 and Injection Kit methods shows greater variability in spring and summer.

Table 4.8. presents the comparative matrix between the measured monthly average vs. the adjusted monthly average for each season and method in Area A.

Table 4.8. Comparative matrix between measured and adjusted monthly averages of CO_2 emissions by the seasonal method for Area A

Area A	Winter		Spring		Summer		Autumn	
	EGM-5	Injection Kit	EGM-5	Injection Kit	EGM-5	Injection Kit	EGM-5	Injection Kit
Average measured values ($g\ m^{-2}h^{-1}$)	0.066	0.052	0.254	0.16	0.882	0.578	0.129	0.113
Adjusted mean ($g\ m^{-2}h^{-1}$)	0.0169	0.0132	0.0653	0.0413	0.2095	0.0524	0.0333	0.029
Average difference between methods (measured values) ($g\ m^{-2}h^{-1}$)	0.014		0.094		0.304		0.016	
Mean difference between methods (adjusted values) ($g\ m^{-2}h^{-1}$)	0.0037		0.024		0.0524		0.0043	
SD (measured values)	0.036	0.023	0.101	0.127	0.063	0.06	0.078	0.084
SD (adjusted values)	0.0092	0.0059	0.0259	0.0327	0.0456	0.0524	0.0201	0.0218

The seasonal distribution of adjusted CO_2 emissions for Area B measured with the EGM-5 and Injection Kit methods shows greater variability in spring and summer.

Table 4.9. presents the comparative matrix between the measured monthly average vs. the adjusted monthly average for each season and method in Area B.

Table 4.9. Comparative matrix between measured and adjusted monthly averages of CO_2 emissions by the seasonal method for Area B

Area B	Winter		Spring		Summer		Autumn	
	EGM-5	Injection Kit	EGM-5	Injection Kit	EGM-5	Injection Kit	EGM-5	Injection Kit
Average measured values (g $m^{-2}h^{-1}$)	0.0278	0.0242	0.0428	0.0407	0.1471	0.1164	0.0321	0.0298
Adjusted mean (g $m^{-2}h^{-1}$)	0.0122	0.0106	0.0187	0.0178	0.0645	0.0108	0.0141	0.013
Average difference between methods (measured values) (g $m^{-2}h^{-1}$)	0.0036		0.0021		0.0307		0.0023	
Mean difference between methods (adjusted values) (g $m^{-2}h^{-1}$)	0.0016		0.0179		0.0537		0.0011	
SD (measured values)	0.0108	0.0118	0.0085	0.0115	0.0378	0.0247	0.0143	0.0137
SD (adjusted values)	0.0047	0.0051	0.0229	0.005	0.0166	0.0108	0.0062	0.006

The seasonal distribution of adjusted CO_2 emissions for Area C measured with the EGM-5 and Injection Kit methods also shows greater variability in spring and summer.

In Table 4.10., the comparative matrix between the measured monthly average vs. the adjusted monthly average for each season and method in Area C is presented.

Table 4.10. Comparative matrix between measured and adjusted monthly averages of CO_2 emissions by the seasonal method for Area C

Area C	Winter		Spring		Summer		Autumn	
	EGM-5	Injection Kit	EGM-5	Injection Kit	EGM-5	Injection Kit	EGM-5	Injection Kit
Average measured values (g $m^{-2}h^{-1}$)	0.0244	0.0201	0.0496	0.0361	0.0903	0.0706	0.0284	0.0237
Adjusted mean (g $m^{-2}h^{-1}$)	0.0122	0.0106	0.0187	0.0178	0.0645	0.051	0.0141	0.013
Average difference between methods (measured values) (g $m^{-2}h^{-1}$)	0.0043		0.0135		0.0198		0.0047	
Mean difference between methods (adjusted values) (g $m^{-2}h^{-1}$)	0.0016		0.0009		0.0135		0.0011	
SD (measured values)	0.0138	0.0129	0.0192	0.0138	0.003	0.0085	0.0129	0.0107
SD (adjusted values)	0.0047	0.0051	0.0037	0.0041	0.0191	0.0166	0.0062	0.006

Table 4.11 presents the average values by season and method in each analyzed area to show the variation in CO_2 emissions, highlighting seasonal variations and differences between areas.

Table 4.11. Summary table of average values of measured vs. adjusted CO_2 emissions by season and method, for each area

Season	Method	Mean (g $m^{-2}h^{-1}$)					
		Area A	Area A*	Area B	Area B*	Area C	Area B*
Winter	EGM-5	0.066	0.0169	0.0278	0.0122	0.0244	0.0122
	Injection Kit	0.052	0.0132	0.0242	0.0106	0.0201	0.0106
Spring	EGM-5	0.254	0.0653	0.0428	0.0187	0.0496	0.0187
	Injection Kit	0.16	0.0413	0.0407	0.0178	0.0361	0.0178
Summer	EGM-5	0.882	0.2095	0.1471	0.0645	0.0903	0.0645
	Injection Kit	0.578	0.0524	0.1164	0.0108	0.0706	0.051
Autumn	EGM-5	0.129	0.0333	0.0321	0.0141	0.0284	0.0141
	Injection Kit	0.113	0.029	0.0298	0.013	0.0237	0.013
*values adjusted according to the particularities of geometry and vegetation distribution							

The EGM-5 method has a higher sensitivity and provides higher values compared to the Injection Kit method, especially in the summer months. The differences vary depending on the season and location, which indicates that for a more accurate estimation of emissions, the EGM-5 method may be more suitable. However, to ensure a higher accuracy of the measurements, it is recommended to use the EGM-5 method and the Injection Kit simultaneously. The complementarity of the two techniques can contribute to a closer assessment of CO_2 emissions in the peri-urban wetland area, to natural phenomena, reducing the uncertainties associated with each method under different seasonal conditions. It is recommended for the warm season, from a daily average temperature of 25°C to use the EGM-5 method, respectively, the equations in Table 4.6 and Table 4.7.

4.4. Methods to improve the estimation of CO_2 emissions from the water-atmosphere interface

It is known that CO_2 emissions are directly dependent on two important factors, namely air temperature (T_{air}) and atmospheric pressure (P*), which can help extrapolate the existing database obtained through discontinuous hourly measurements.

The extrapolation of CO_2 emissions for 2022 was carried out based on T_{air} and P* for each location in the study area because both measurement methods depend on these climate parameters. For a better estimate of the actual CO_2 emissions in the extrapolation, the monthly average emissions were adjusted, taking into account the differences in emissions between day and night based on the measurements taken to determine the variations. Thus, the monthly average CO_2 emissions were weighted by introducing a coefficient based on the duration of the day and night hourly intervals specific to each month. The values are adjusted based on the hypothesis that takes into account the day and night variation, highlighting significant variations at the seasonal level and providing more precise estimates.

Figure 4.11 shows the extrapolated and corrected CO_2 emission values obtained by the EGM-5 method and the Injection Kit method for the 3 locations.

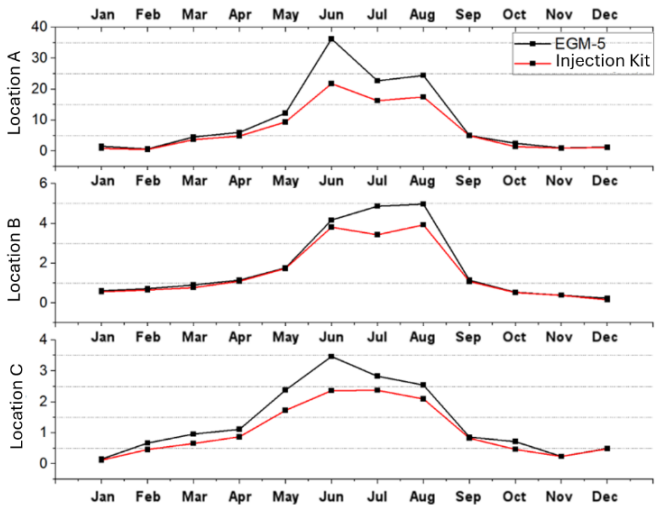


Fig. 4.11. CO_2 emission values extrapolated and adjusted based on day-night variation obtained by the EGM-5 method and the Injection Kit method for Locations A, B, and C

There is an interdependence between the measurement methods used to determine CO_2 emissions in the investigated locations, so that statistical-mathematical models can be developed for peri-urban wetlands. The statistical-mathematical models regarding the correlation between the extrapolated CO_2 emissions for the two measurement methods are centralized and presented in Table 4.12 and show a very strong correlation [59] in all three analyzed locations r(0.986÷0.998), respectively, with S(0.136÷0.854).

Table 4.12. Statistical-mathematical models regarding the correlation between extrapolated CO_2 emissions for the EGM-5 and Injection Kit measurement methods in the three locations

Location	Independent variable	S	r	Regression equation
A	EGM-5	0.419	0.998	$a=0.891b+0.0078b^2$
	Injection Kit	0.854	0.997	$b=0.957a+0.029a^2$
B	EGM-5	0.184	0.992	$a=1.046b-0.054b^2$
	Injection Kit	0.287	0.988	$b=1.048a+0.0508a^2$
C	EGM-5	0.136	0.987	$a=0.0.858b-0.037b^2$
	Injection Kit	0.192	0.986	$b=1.259a+0.0125a^2$
a=EGM-5 method b=Injection Kit method				

In order to ensure a high level of confidence in the CO_2 emissions over the entire wetland, extrapolation was proposed by introducing an adjustment coefficient that takes into account the particularities of the investigated areas, presented in Chapter 3.2.

Figure 4.12 shows the extrapolated and corrected CO_2 emission values obtained by the EGM-5 method and the Injection Kit method for the 3 areas. Area A continues to show the largest differences between the two models in the summer months, while for Area B and Area C, the differences between the extrapolated values for the two methods are much smaller.

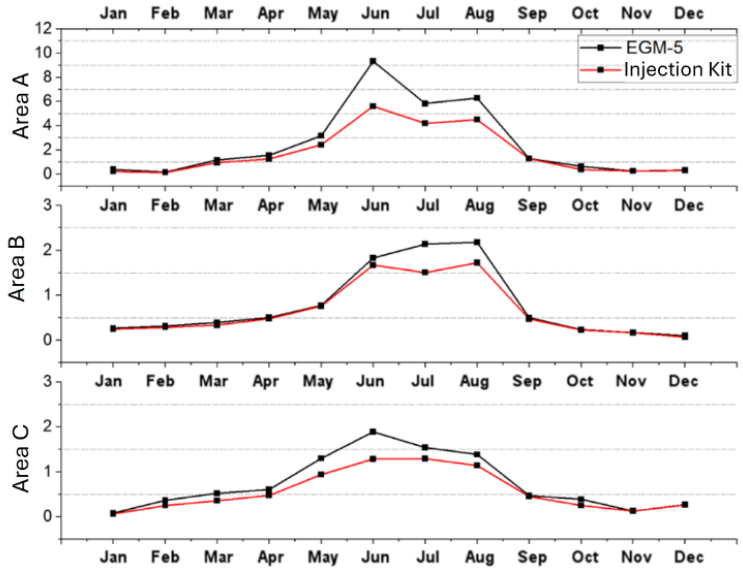


Fig. 4.12 Extrapolated and corrected CO_2 emission values obtained by the EGM-5 method and the Injection Kit method for Areas A, B, and C

The Pearson correlation shows for the extrapolated values of the two methods in Area A a coefficient of 0.991 ($p<0.01$), for Area B 0.988; ($p<0.01$), and for Area A 0.986; ($p<0.01$).

The statistical-mathematical models regarding the correlation between CO_2 emissions extrapolated according to the geometric features and distribution of vegetation for the two measurement methods are centralized and presented in Table 4.13 and show a very strong correlation [59] in all three analyzed areas r(0.986÷0.998), respectively, with S(0.081÷0.287).

Table 4.13. Statistical-mathematical models regarding the correlation between extrapolated CO_2 emissions for the EGM-5 and Injection Kit measurement methods in the three areas

Location	Independent variable	S	r	Regression equation
A	EGM-5	0.108	0.998	$a=0.891b-0.0307b^2$
	Injection Kit	0.220	0.997	$b=0.957a+0.1154a^2$
B	EGM-5	0.081	0.992	$a=1.046b-0.054b^2$
	Injection Kit	0.287	0.988	$b=1.048a+0.1156a^2$
C	EGM-5	0.104	0.986	$a=0.1.259b-0.0408b^2$
	Injection Kit	0.192	0.986	$b=1.259a+0.0125a^2$
a=EGM-5 method b=Injection Kit method				

In conclusion, based on the regression equations and considering the interdependence of the methods, it is recommended to continue using the EGM-5 method (which is based on the principle of an air collection pump, suitable for dynamic measurements). In situations where only measurements made with the Injection Kit method are available, it is recommended to apply the relationships presented in Table 4.13., since the statistical-mathematical models included are more general and have a high level of confidence, independent of factors such as temperature, pressure, day-night variations, or the geometric particularities of the area.

4.5. CO_2 emissions measured in-situ at the soil-atmosphere interface with the EGM-5 method

The variations in CO_2 emissions for the SC and SP locations (Figure 4.13) show differences in the dynamics of monthly emissions. During the period January-April, the SC Location has slightly higher emission values than the SP Location, but their magnitude remains low. Starting with May, the differences between the locations become more evident, with the SC Location recording 0.5716 g m^{-2} h^{-1}, while the SP Location recorded a maximum of 0.2883 g g m^{-2} h^{-1}. In August, the SP Location reached a maximum emission of 1.375 g m^{-2} h^{-1}, compared to the SC Location, where 0.2839 g m^{-2} h^{-1} were recorded. This is the most significant difference between the locations during the year, with the SP Location having considerably higher emissions than the SC Location. Starting with September, emissions from the SC Location remain moderate, while emissions from the SP decrease sharply, reaching a minimum of 0.0612 g m^{-2} h^{-1} in December.

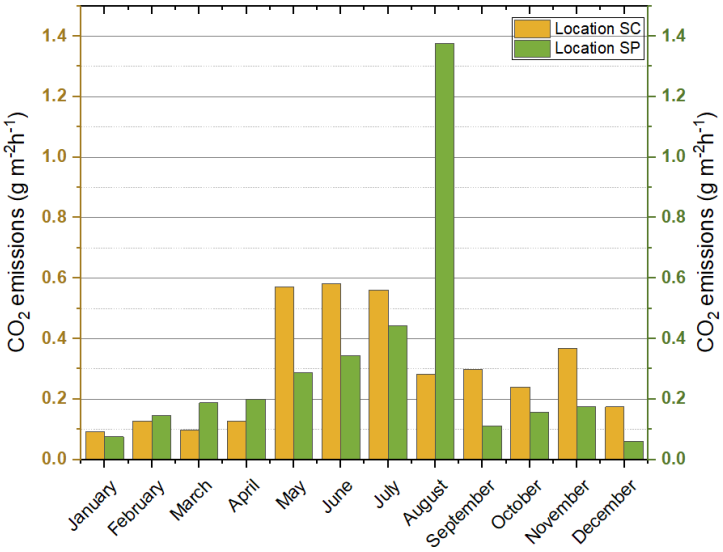


Fig. 4.13. Spatial and temporal variation of CO_2 emissions from the land surface to the atmosphere

Table 4.14 summarizes the Pearson correlation coefficient, t-test results, and ANOVA for the average annual differences in CO_2 emissions from Location SC and Location SP.

Table 4.14. Results of Pearson correlation coefficient, t-test, and ANOVA for mean differences in CO_2 emissions from Location SC and Location SP

Pearson correlation coefficient		T-test			ANOVA	
r	p	Annual average difference (g m^{-2} h^{-1})	t	p (Sig.)	F	p (Sig.)
0.880	0.009	0.067	1.209	0.272	0.422	0.528

The location-specific variations reflect differences in the intensity and rhythm of soil metabolic activities throughout the year, with Location SC showing more stable activity, while Location SP shows more pronounced fluctuations. However, at the annual level, the t-test

(t=1.209; p=0.272) and ANOVA analysis (F=0.422; p=0.528) indicate the lack of a statistically significant difference between locations.

4.6. Temporal and spatial dynamics of CO_2 emissions from the water-atmosphere interface

4.6.1. Analysis of the temporal variability of the CO_2 flux from the water-atmosphere interface considering spatial variability

The monthly variations of CO_2 emissions using the extrapolated values from Table 4.32 for the EGM-5 method applied in Area A, B, and C are shown in Figure 4.14. Between January and May, the average emissions gradually increase, indicating a gradual increase in biological activities. Between June and August, emissions register a significant increase in all areas, with notable values in June for Area A, when emissions reach 9.33 g m^{-2} day^{-1}. Starting in September, CO_2 emissions show a gradual decrease, although they remain relatively high compared to the beginning of the year.

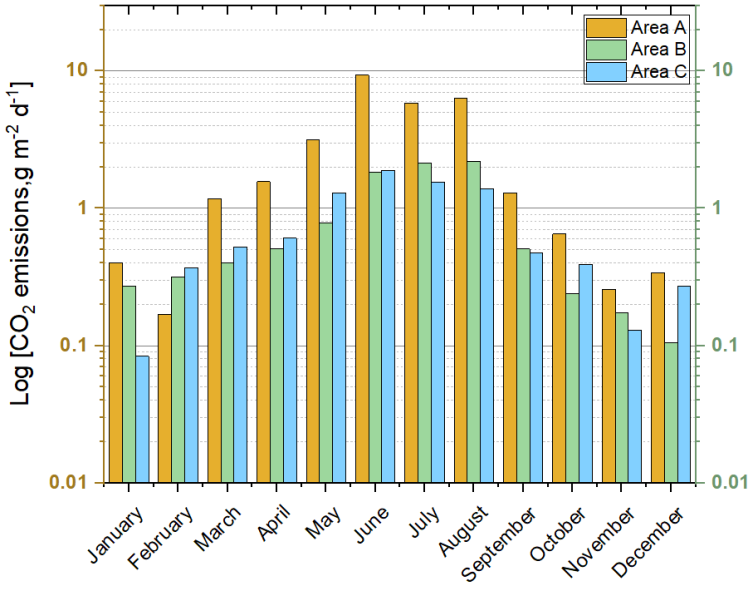


Fig. 4.14. Monthly and spatial variation of CO_2 emissions by area

Statistical-mathematical models were developed that are generally valid for the entire area of the investigated wetland at an annual level. Table 4.15 presents the statistical-mathematical correlations for CO_2 emissions as a function of T_{air} and P* in each of the three areas, where the correlation coefficient is r(0.855÷0.955) and the standard error is S(0.332÷5.149).

Table 4.15. Regression models between CO_2 emissions and the main meteorological parameters in the investigated areas

Regression model	Statistical parameter	Area A	Area B	Area C
Simple regression E=f(T)	**R^2**	0.864	0.874	0.857
	Eq.	$E= 8.72T-0.677T^2$	$E= 27.7T-7.27T^2$	$E=25.3T-6.28T^2$
	SD	5.026	4.847	5.149
Simple regression E=f(P*)	**R^2**	0.864	0.955	0.855
	Eq.	$E=-33.18P^*+1110.4\ P^{*2}$	$E=5.796P^*-1.293P^{*2}$	$E=36.29P^*-88.13P^{*2}$
	SD	1.587	0.932	0.332
Multiple	**R^2**	0.809	0.873	0.891

regression	**Eq.**	E=0.257T−0.088P*	E=0.71T-0.015P*	E=0.054T-0.002P*
E=f(T,P*)	**SD**	1.840	0.425	0.342
P=P/1000*				

To estimate CO_2 emissions from the water-atmosphere interface in periurban wetlands, it is recommended to use the regression equation (4.1.), which takes into account both the day-night variation and the overall geometric shape and spatial distribution of vegetation.

$$E=0.613T-0.009P^* \quad (4.1.)$$

4.7. Temporal and spatial dynamics of CO_2 emissions from the soil-atmosphere interface

4.7.1. Analysis of the temporal variability of the CO_2 flux from the soil-atmosphere interface as a function of spatial variability and vegetation distribution

Monthly variations in CO_2 emissions using previously extrapolated values for the SC and SP Locations are shown in Figure 4.15 [59].

Between January and April, both locations record low CO_2 emissions. The values increase until April, indicating increasing biological activity in both locations. Starting in May, the SC Location records one of its annual maxima, reaching a value of 18.99 g m-2 day-1, while the SP Location records only 9.58 g m-2 day-1, a significant difference that indicates a more intense microbial activity or more favorable local conditions in the SC Location, which favor high CO_2 emissions. In June, the SC Location reaches the maximum value of the year of 22.58 g m-2 day-1, while the SP Location records the highest emissions in August, with a value of 37.35 g m-2 day-1. Starting from September until the end of the year, CO_2 emissions gradually decrease in both locations. The t-test (t=1.205, p=0.274) indicates the lack of a significant difference between locations, and the ANOVA analysis (F=0.361, p=0.559) supports these results.

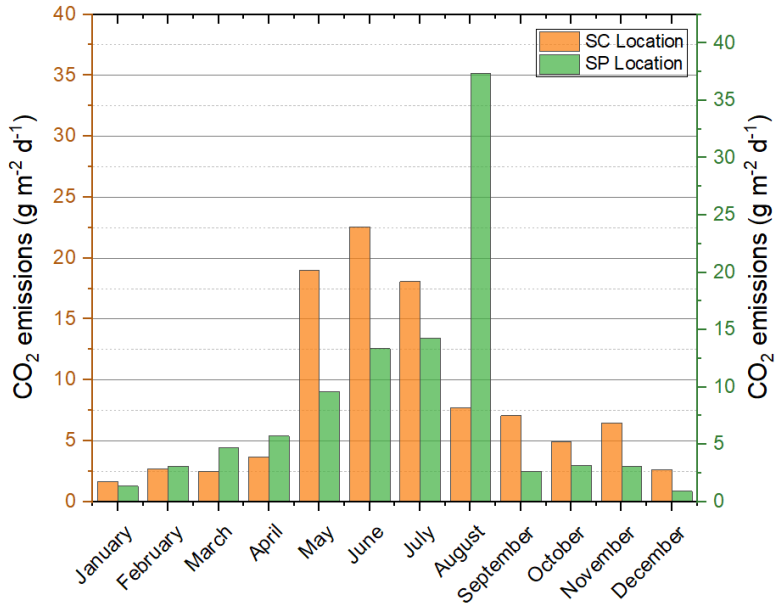
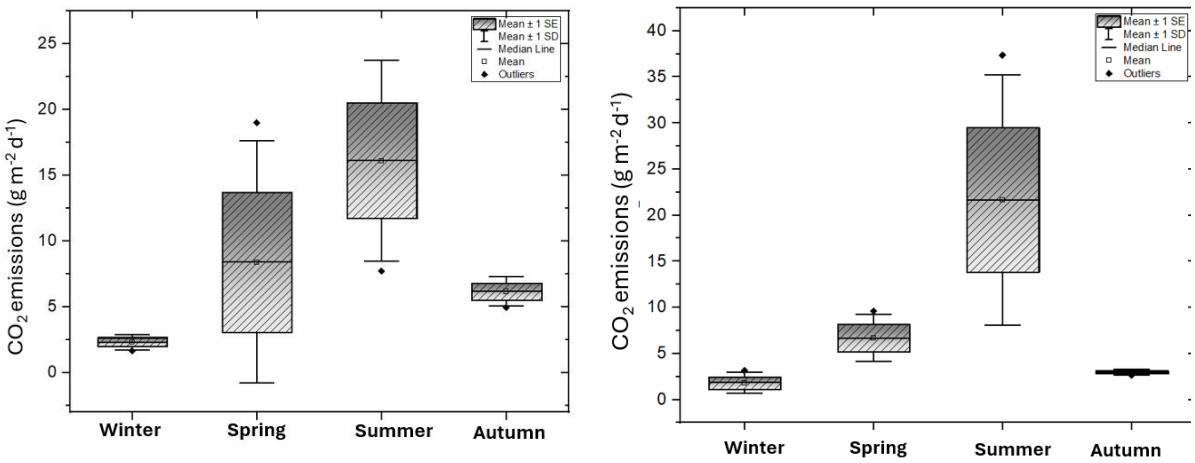


Fig. 4.15. Monthly variation of CO_2 emissions measured in SC and SP Locations



a) b)

Fig. 4.16. Seasonal variation of CO_2 emissions measured in Locations SC (a)) and SP (b))

The differences between the two locations show higher averages in winter and spring, but with different variability in the SC Location, while the SP Location has lower and more stable emissions. In summer, CO_2 emissions were considerably higher in the SP Location compared to the SC Location, due to the soil flooding event, but the observed differences were not confirmed by the t-test and ANOVA analysis, which indicated a lack of statistical significance.

Statistical-mathematical models were developed that are generally valid for CO_2 emissions from the soil-atmosphere interface, depending on the main dependent parameters. Table 4.16 presents the statistical-mathematical correlations for CO_2 emissions as a function of T_{air}, T_{soil}, P*, and M_{soil} in the SC and SP Locations, where the correlation coefficient is r(0.823÷0.955) as well as the standard error of S(0.004÷5.277). To estimate CO_2 emissions from the soil-atmosphere interface according to the main parameters, it is recommended to use the regression equations presented in Table 4.16. The general equation for soils depends on the soil type, which implies a deeper analysis in this regard.

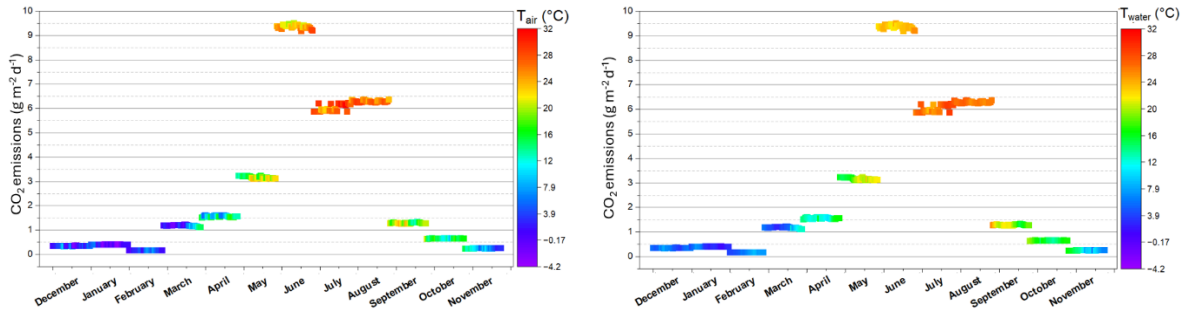
Table 4.16. Statistical-mathematical models regarding the relationship between CO_2 emissions and the main physical parameters of the soil for SC and SP

Parameter		SC	SP
Simple regression $E=f(T_{air})$	R^2	0.873	0.849
	Eq.	$E= 2.94\ T_{air} -0.087T_{air}^2$	$E= 2.49\ T_{air}-0.047T_{air}^2$
	SD	4.865	5.277
Simple regression $E=f(T_{soil})$	R^2	879	0.908
	Eq.	$E= 2.81T_{soil}-0.09T_{soil}^2$	$E= 2.99T_{soil}-0.06T_{soil}^2$
	SD	3.640	3.259
Simple regression $E=f(P^*)$	R^2	0.872	0.850
	Eq.	$E= 2.81T_{soil}-0.09T_{soil}^2$	$E= 2.48T_{soil}-0.004T_{soil}^2$
	SD	0.004	0.005
Simple regression $E=f(M_{soil})$	R^2	0.823	0.955
	Eq.	$E= -0.41M_{soil}+0.014M_{soil}^2$	$E= 4.35M_{soil}-0.08M_{soil}^2$
	SD	4.371	4.699
Multiple regression $E=f(T_{air},T_{soil})$	R^2	0.908	0.842
	Eq.	$E= 0.77T_{air}-0.188T_{soil}$	$E= 0.880T_{air}-0.219T_{soil}$
	SD	1.582	2.457
Multiple regression $E=f(T_{air},T_{soil},P^*)$	R^2	0.910	0.847
	Eq.	$E= 1.05T_{air}-0.62T_{soil}+1.81P^*$	$E= 0.855T_{air}-0.137T_{soil}-1.07P^*$
	SD	1.423	2.352
Multiple regression $E=f(T_{air},T_{soil},P^*,M_{soil})$	R^2	0.916	0.941
	Eq.	$E= 3.75T_{air}+0.21T_{soil}+0.032P^*+0.003M_{soil}$	$E= 1.51T_{air}-1.9T_{soil}+12.8P^*+0.34M_{soil}$
	SD	1.354	0.865
$P^*=P/1000$			

4.8. Analysis of the dependence of CO_2 emissions on the main parameters

4.8.1.1. Analysis of the dependence of CO_2 emissions from the water-atmosphere interface on the main parameters

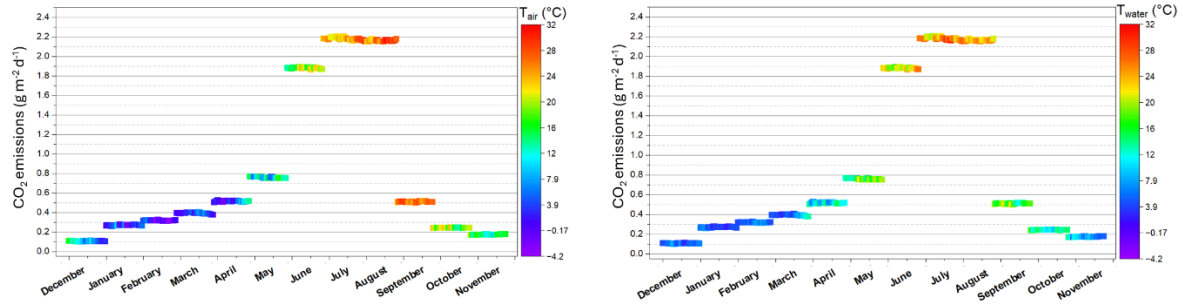
The following graphs in Figure 4.17 present the daily average values of CO_2 emissions in relation to T_{air} and T_{water} variables for Area A [21]. The variation of CO_2 emissions follows similar trends to those of temperatures. As temperatures increase, CO_2 emissions also increase, reaching values of up to 3.16 g m^{-2} d^{-1} at T_{air} and T_{water} values of 23°C in May. Between June and August, at temperatures exceeding 30°C, higher CO_2 emissions of up to 9.33 g m^{-2} d^{-1} were observed, demonstrating that this period is the most intense for CO_2 emissions from the water-atmosphere interface, strongly influenced by T_{air} and T_{water} values. The Pearson coefficient correlations between CO_2 emissions and temperatures proved to be strongly positive and statistically significant [59] with r=0.813; p<0.01 for T_{air} and r=0.764; p<0.01 for T_{water}.



a) b)

Fig. 4.17. Variation of CO_2 emissions from the water-atmosphere interface and the average daily air temperature (T_{air}) and soil temperature (T_{water}) in Area A

The graphs in Figure 4.18 show the variation of CO_2 emissions as a function of T_{air} and T_{water} for Area B [210]. It is observed that CO_2 emissions increase with temperature, the maximum values being recorded during the summer. In the period June-August, CO_2 emissions reach the highest values under T_{air} and T_{water} conditions with values between 21.3°C and 32°C, recording a maximum of emissions of 2.832 g m^{-2} d^{-1}. The Pearson coefficient correlations between CO_2 emissions and temperatures proved to be strongly positive and statistically significant [59] with r=0.857; p<0.01 for T_{air} and r=0.742; p<0.01 for T_{water}.

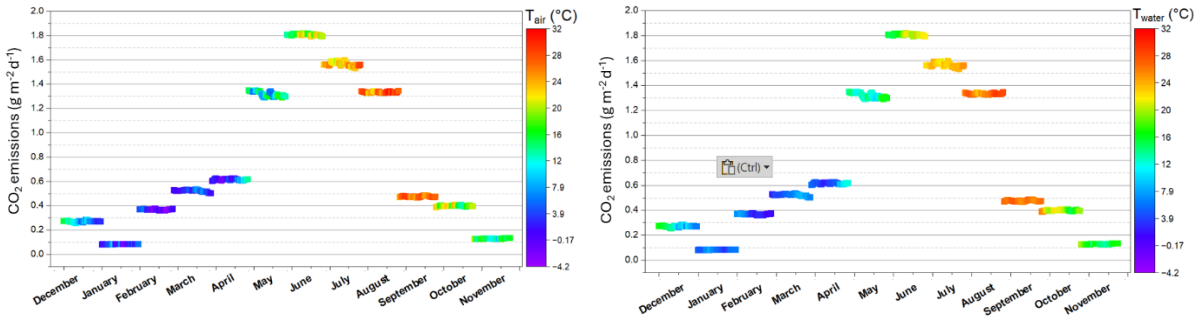


a) b)

Figure. 4.18. Variation of CO_2 emissions from the water-atmosphere interface and the average daily air temperature (T_{air}) and soil temperature (T_{water}) in Area B

CO_2 emissions by T_{air} and T_{water}, for Area C, presented in Figure 3.19 reflect their dependence [59]. In the winter months, when the values are lowest, CO_2 emissions remain at a minimum level in the area. With the increase in temperatures, in the period June-August, when

T_{air} and T_{water} reach maximum values above 32°C, CO_2 emissions are also the highest, presenting values of up to 1.89 g m^{-2} d^{-1}. The Pearson coefficient correlations between CO_2 emissions and temperatures proved to be strongly positive and statistically significant [59] with r=0.845; p<0.01 for T_{air} and r=0.894; p<0.01 for T_{water}.



a) b)

Fig. 4.19. Variation of CO_2 emissions from the water-atmosphere interface and the average daily air temperature (Tair) and soil temperature (Twater) in Area C

Table 4.17 summarizes the results of the regression coefficient between CO_2 emissions from the water-atmosphere interface and dependent meteorological and physical parameters in the three analyzed areas.

Table 4.17. Statistical-mathematical models regarding the relationship between CO_2 emissions from the water-atmosphere interface and the main dependent meteorological and physical parameters

Area	Variable	R^2	Regression equation	SD
A	$E=f(T_{air})$	0.792	$E=0.211T_{air}$	0.044
	$E=f(T_{water})$	0.696	$E=0.2.12T_{water}$	0.049
	$E=f(Pp)$	0.263	*neconcludent*	0.332
	$E=f(VV)$	0.504	*neconcludent*	0.008
	$E=f(T_{air}, T_{water})$	0.794	$E=0.247T_{air}$ -0.039$_{wtaer}$	0.118
	$E=f(T_{air}, T_{water}, Pp)$	0.802	$E=0.229T_{air}$-0.014T_{water}-0.085Pp	0.359
	$E=f(T_{air}, T_{water}, Pp, VV)$	0.820	$E=0.277T_{air}$-0.138T_{wtaer}-0.136 Pp +0.651VV	1.369
B	$E=f(T_{air})$	0.866	$E=0.063T_{air}$	0.008
	$E=f(T_{water})$	0.768	$E=0.062T_{wtaer}$	0.010
	$E=f(Pp)$	0.048	*neconcludent*	0.132
	$E=f(VV)$	0.439	*neconcludent*	0.334
	$E=f(T_{air}, T_{water})$	0.874	$E=0.085T_{air}$-0.025T_{wtaer}	0.085
	$E=f(T_{air}, T_{water}, Pp)$	0.903	$E=0.093T_{air}$-0.028T_{wtaer} -0.070Pp	0.331
	$E=f(T_{air}, T_{water}, Pp, VV)$	0.920	$E=0.116T_{air}$-0.067T_{wtaer} -0.104Pp +0.155VV	0.155
C	$E=f(T_{air})$	0.891	$E=0.055T_{air}$	0.055
	$E=f(T_{water})$	0.907	$E=0.052T_{wtaer}$	0.052
	$E=f(Pp)$	0.189	*neconcludent*	0.073
	$E=f(VV)$	0.460	*neconcludent*	0.300
	$E=f(T_{air}, T_{water})$	0.909	$E=0.015T_{air}$-0.039T_{wtaer}	0.020
	$E=f(T_{air}, T_{water}, Pp)$	0.916	$E=0.019T_{air}$+0.036T_{wtaer}-0.020Pp	0.209
	$E=f(T_{air}, T_{water}, Pp, VV)$	0.943	$E=-0.02T_{air}$+0.088T_{wtaer}+0.008Pp -0.175VV	1.621

For a more precise explanation of emissions from the water-atmosphere interface, the values of water quality parameters from each study area were involved. Thus, Pearson correlation coefficient, as well as simple regressions, were used for statistical analysis for each area. CO_2 emissions at the area level show significant correlations with several water quality parameters measured in-situ [60]. In Area A, the strongest correlations occur between CO_2 emissions and chlorophyll (r=0.903), ORP (r=0.854), and a negative but highly significant correlation with pH, with r=-0.885; p<0.01. Areas B and C show similar trends with significant correlations and high values of the coefficient of determination (R^2 between 0.722 and 0.815). Also, DO shows a moderate positive correlation in all areas.

Statistical-mathematical models regarding the correlation between monthly averages of CO_2 emissions and water quality parameters are presented in Table 4.18 and show a very strong correlation in all three areas.

To estimate CO_2 emissions from the water-atmosphere interface in peri-urban wetlands, it is recommended to use the regression equation (4.2.), which considers both the spatial distribution of vegetation and the main water quality parameters.

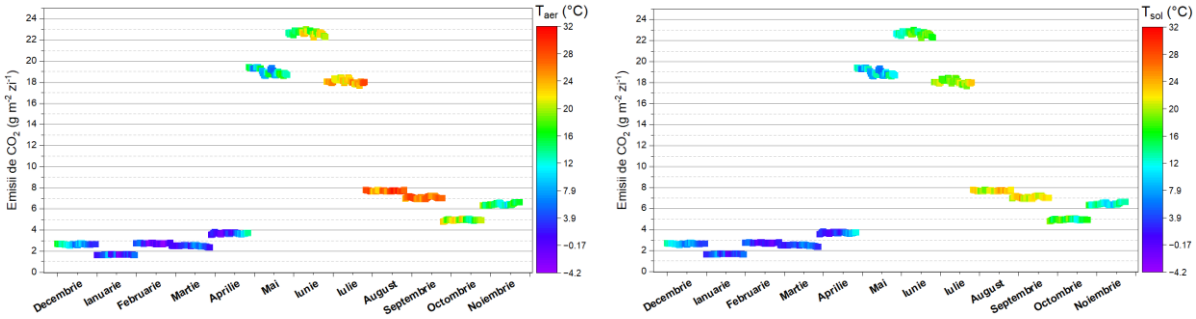
$$E = 0.036pH + 0.016ORP + 1.141C^* - 0.058DO + 0.118T_{water} \quad (4.2)$$

Table 4.18. Multiple statistical-mathematical models regarding the relationship between CO_2 emissions from the water-atmosphere interface and the main water quality parameters

Area	Model		
A	*E=f(pH, ORP)*	R^2	0.923
		Eq.	$E = 0.087pH + 0.019ORP$
		SD	1.68
	E=f(pH, ORP, C)*	R^2	0.95
		Eq.	$E = -0.93pH + 0.008ORP + 1.141C^*$
		SD	1.213
	E=f(pH, ORP, C, DO)*	R^2	0.957
		Eq.	$E = 0.077pH + 0.014ORP + 1.402C^* - 0.041DO$
		SD	1.5
B	*E=f(pH, ORP)*	R^2	0.952
		Eq.	$E = 0.014pH + 0.008ORP$
		SD	2.061
	E=f(pH, ORP, C)*	R^2	0.958
		Eq.	$E = -0.57pH + 0.006ORP + 0.244C^*$
		SD	1.823
	E=f(pH, ORP, C, DO)*	R^2	0.959
		Eq.	$E = -0.45pH + 0.006ORP + 0.134C^* - 0.004DO$
		SD	1.483
C	*E=f(pH, ORP)*	R^2	0.865
		Eq.	$E = 0.070pH + 0.003ORP$
		SD	1.38
	E=f(pH, ORP, C)*	R^2	0.964
		Eq.	$E = -0.039pH + 0.001ORP + 0.245C^*$
		SD	2.094
	E=f(pH, ORP, C, DO)*	R^2	0.966
		Eq.	$E = -0.048pH + 0.001ORP + 0.196C^* - 0.004DO$
		SD	1.911

4.8.2. Analysis of the dependence of CO_2 emissions from soil on the main parameters

The relationship between T_{air}, T_{soil}, and CO_2 emissions from the SC Location, presented in Figure 4.20, shows a dependence between these variables. In winter, at temperatures close to zero, CO_2 emissions are minimal (1.66 g m^{-2} d^{-1}) due to the inhibition of microbial activity. With the increase of T_{air} and T_{soil} above 10–15 °C, emissions increase significantly, reaching 18.98 g m^{-2} d^{-1} at above 19 °C. In summer, at T_{air}>30 °C, they reach a maximum of 22.58 g m^{-2} day^{-1} and remain constant. Subsequently, with the decrease in temperatures, emissions gradually decrease, but remain higher than in winter. The Pearson coefficient correlations between CO_2 emissions from the soil-atmosphere interface and T_{air}, T_{soil} from the SC Location proved to be strongly positive and statistically significant.



a) b)

Fig. 4.20. Variation of the monthly average of measured CO_2 emissions and the daily average of T_{air} (a) and T_{soil} (b) for the SC Location

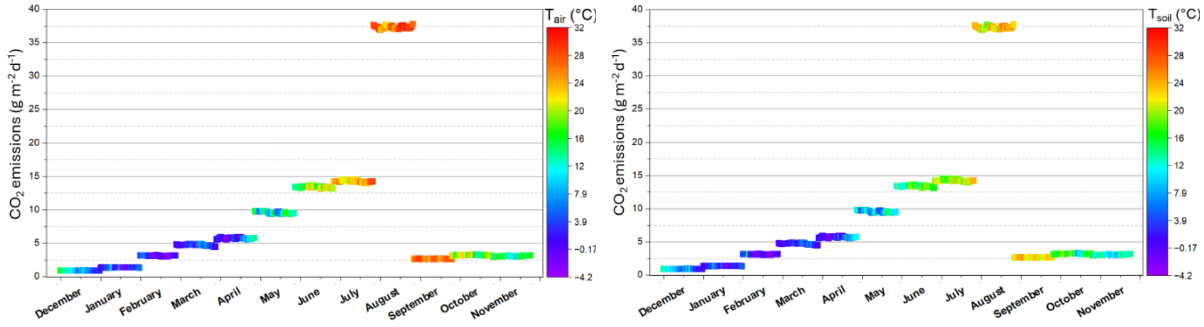
In order to highlight the dependency relationship between CO_2 emissions and the main climate factors in the SC Location, statistical-mathematical models were developed that are generally valid for the SC Location in the investigated wetland. Table 4.19 presents the statistical-mathematical correlations between CO_2 emissions and dependent meteorological parameters.

Table 4.19. Statistical-mathematical models regarding the relationship between CO_2 emissions and the main physical parameters in the SC Location

Variable	R^2	Regression equation	SD
$E=f(T_{air})$	0.823	$E=0.608T_{air}$	0.085
$E=f(T_{soil})$	0.803	$E=0.686T_{soil}$	0.102
$E=f(M_{soil})$	0.687	$E=0.223M_{soil}$	0.045
$E=f(Pp)$	0.763	$E=0.958Pp$	0.152
$E=f(VV)$	0.391	unconclusive	1.004
$E=f(T_{air}, T_{soil})$	0.824	$E=0.771T_{air}$ -0.188T_{soil}	0.824
$E=f(T_{air}, T_{soil}, M_{soil})$	0.824	$E=0.799T_{air}$-0.247T_{soil}+0.010M_{soil}	0.687
$E=f(T_{air}, T_{soil}, M_{soil}, Pp)$	0.876	$E=-0.51T_{air}$+1.33T_{soil}-0.186M_{soil}+0.725Pp	0.763
$E=f(T_{air}, T_{soil}, M_{soil}, Pp, VV^*)$	0.879	$E=-0.408T_{air}$+1.22T_{soil}-0.229M_{soil}+0.77Pp-0.572VV	0.824

The variation of CO_2 emissions as a function of T_{air} for the SP Location, represented in Figure 4.21, highlights a strong positive relationship. In winter, emissions are minimal (0.92 g m^{-2} d^{-1}). Between March and May, with the increase of T_{air} up to 23.58 °C, they increase progressively up to 9.58 g m^{-2} d^{-1}. In summer (June–July), at T_{air} of 32.02 °C, emissions reach 14.25 g m^{-2} d^{-1}, and in August, the maximum values of the SP Location (37.35 g m^{-2} d^{-1}). From September, emissions gradually decrease with the decrease in temperatures. The Pearson

correlation between emissions and T_{air} is strongly positive and statistically significant (r=0.852; p<0.01), and between emissions and T_{soil} is r=0.842; p<0.01.



a) b)

Fig. 4.21. Variation of the monthly average of measured CO_2 emissions and the daily average of T_{air} (a) and T_{soil} (b) for the SP Location

The variation of CO_2 emissions and Pp (7 days) from the SP Location (Figure 4.22) highlights an influence of precipitation on CO_2 emissions, but also a specific seasonal variation, influenced by other factors such as temperature.

At the beginning of the year, precipitation is low (0.425–2.56 mm/day) and corresponds to the minimum CO_2 emissions. Between May and August, they increase significantly, reaching maximums in August (17.63–18.72 mm/day). Subsequently, emissions decrease in September with the reduction of temperatures and the frequency of Pp (7 days). In November–December, emissions reach annual minima, while Pp (7 days) remains moderate (≤5.32 mm/day). The Pearson correlation between emissions and Pp (7 days) is strongly positive and significant (r=0.936; p<0.01).

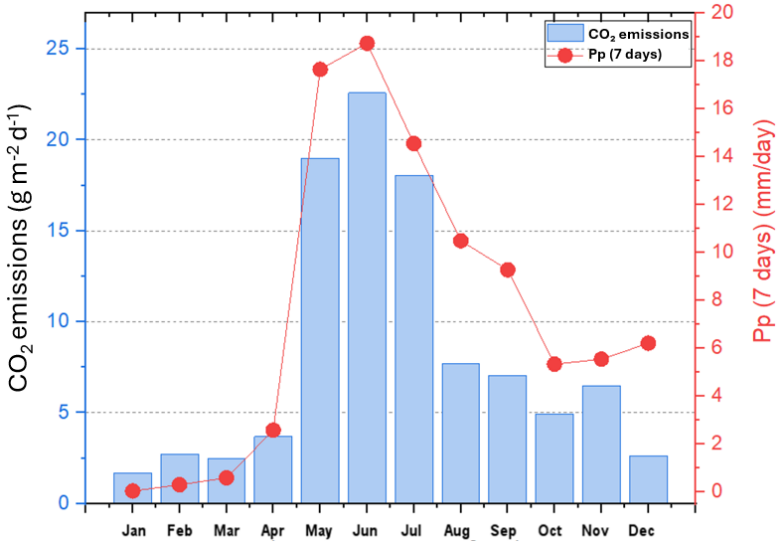


Fig. 4.22. Variation between CO_2 and Pp emissions (7 days) in the SP Location

In order to highlight the dependency relationship between CO_2 emissions and the main climatic and physical, and soil factors in the SP Location, statistical-mathematical models were developed that are generally valid on the SP Location in the investigated wetland. Table 4.20 presents the statistical-mathematical correlations between CO_2 emissions and dependent meteorological parameters.

Table 4.20. Statistical-mathematical models regarding the relationship between CO_2 emissions and the main physical parameters in the SP Location

Variable	R^2	Regression equation	SD.
T_{air}	0.843	E=0.608T_{air}	0.379
T_{soil}	0.820	E=0.686T_{soil}	0.594
M_{soil}	0.841	E=0.180M_{soil}	0.936
Pp (7 zile)	0.876	E=0.601Pp	0.601
VV	0.532	unconclusive	7.956
$E=f(T_{air}, T_{soil})$	0.991	E=0.359T_{air}+0.162T_{soil}	0.766
$E=f(T_{air}, T_{soil}, M_{soil})$	0.992	E=0.360T_{air}+0.184T_{soil}-0.014M_{soil}	1.404
$E=f(T_{air}, T_{soil}, M_{soil}, Pp)$	0.997	E=0.435T_{air}+0.258T_{soil}-0.027M_{soil}-0.166Pp	1.712
$E=f(T_{air}, T_{soil}, M_{soil}, Pp, VV^*)$	0.998	E=0.394T_{air}+0.329T_{soil}-0.008M_{soil}-0.205Pp-0.402VV	0.911

To estimate CO_2 emissions from the soil-atmosphere interface based on the main dependent meteorological and physical parameters, it is recommended to use the regression equations presented in Table 4.19 and Table 4.20. To estimate with the highest possible level of confidence the total CO_2 emissions from the soil-atmosphere interface related to the periurban wetland, it is necessary to characterize the soil type over the entire area of interest.

4.9. Determination of the degradability rate of surface vegetation

The study investigated how the decomposition of surface vegetation could contribute to the carbon cycle in the study area. For this, we used the litter bag method, which allowed for the direct measurement of the degradability rate under the conditions specific to the study area [61].

4.9.1. Determination of the degradability rate of the *Phragmites australis* species

Figure 4.23 shows the mass values of *Phragmites australis* litter after its collection from the study area and the labile fraction of the material. An initial phase of rapid decomposition occurred in the first 10 days. This was followed by a long phase of relative inhibition of decomposition between days 10-30. Finally, a third stage consisted of significant mass loss that occurred as a result of massive deposition of organic material and invertebrate microorganisms on the bags.

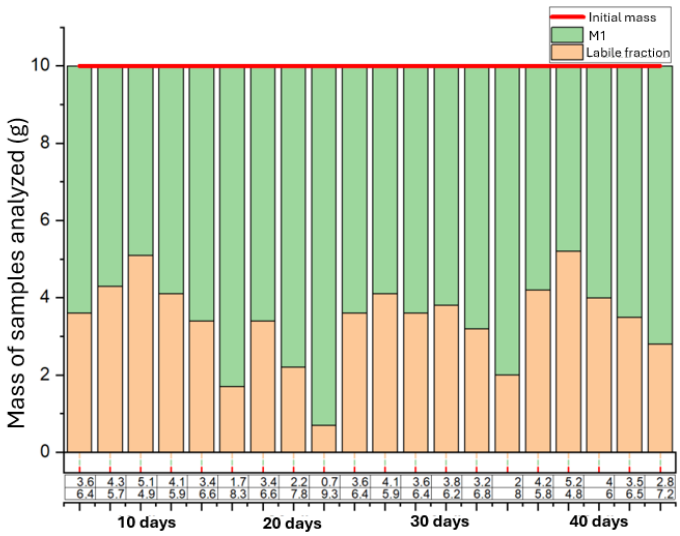


Fig. 4.23. Values of labile fraction (active C) and litter mass collected for the species *Phragmites australis*

The graph in Figure 4.24 shows the values of the recalcitrant fraction and the final mass of the litter after oven drying. Thus, the recalcitrant fraction had values between 1.2g and 0.7g in the first 20 days, and in the last 20 days it stabilized at values between 0.3g and 0.5g. The last stage of stabilization of the recalcitrant fraction indicates that the inactive carbon fraction in the litter can be affected by the input of deposited organic material and making it difficult to predict the long-term impact of this input on C stocks.

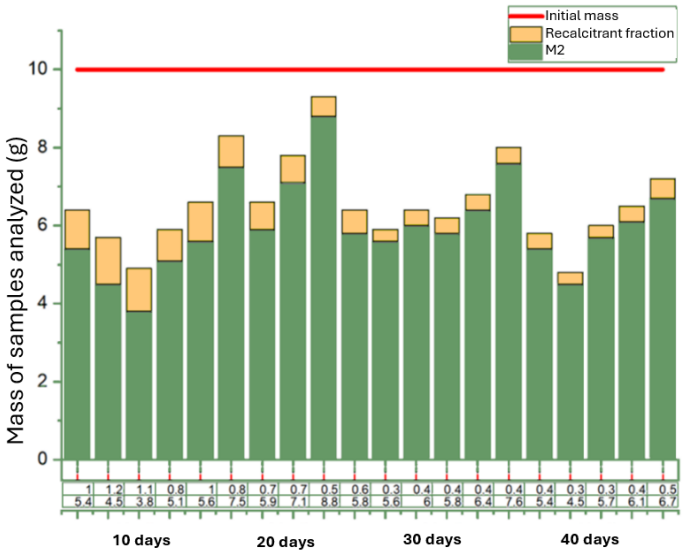


Fig. 4.24. Values of the recalcitrant fraction (C recalcitrant) and of the final litter mass for the species *Phragmites australis*

The graph in Figure 4.25 shows the proportions of active and recalcitrant C reservoirs in the litter formed by the species *Phragmites australis*. The labile fraction constitutes the largest proportion of the total organic carbon (TOC) of the litter. Recalcitrant C, although varying in the first phase, between days 10-20, having increased values compared to the entire series of determinations, then stabilizes at constant values, representing a small percentage of the total fraction.

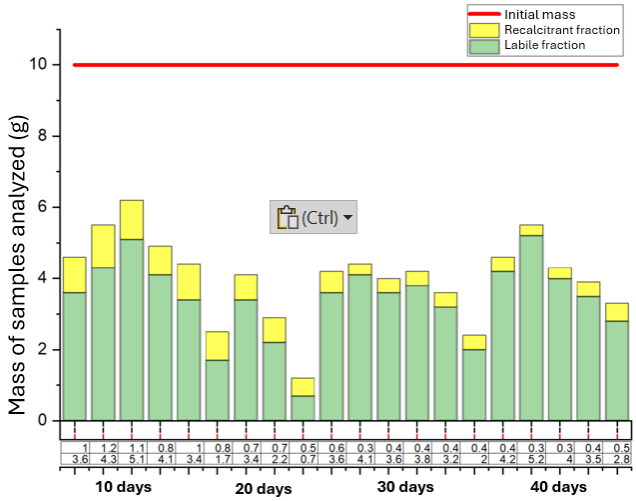


Fig. 4.25. Total organic carbon in the litter formed by the species *Phragmites australis*

Quantification of the labile fraction and the recalcitrant fraction estimated the average total mass loss of the amount of litter studied, which is composed of 3.425 g of active fraction

and 0.61g of recalcitrant fraction.

4.9.2. Determination of the degradability rate of the *Typha latifolia* species

Figure 4.26 shows the litter mass values after collection from the study area and the labile fraction of the material. An initial phase of slow decomposition was in the first 10 days, followed by a long phase of rapid decomposition that occurred between days 20 and 30. Finally, a third stage consisted of uneven mass loss within the collected series, with the labile fraction having a maximum value of 4.7g down to 2g in the 40 days.

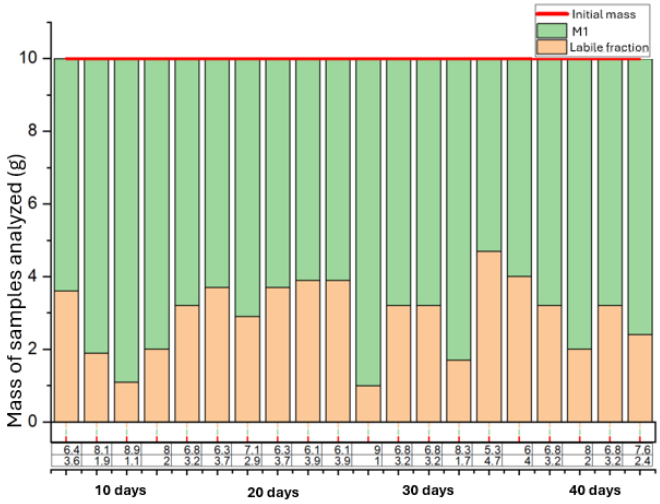


Fig. 4.26. Values of labile fraction (active C) and litter mass collected for the species *Typha latifolia*

The graph in Figure 4.27 shows the proportions of active and recalcitrant C reservoirs in the litter formed by the species Typha latifolia. The labile fraction constitutes the largest proportion of the litter TOC. Recalcitrant C, although varying in the first phase, between days 10-20, having increased values compared to the entire series of determinations, then stabilizes at constant values, representing a small percentage of the total fraction.

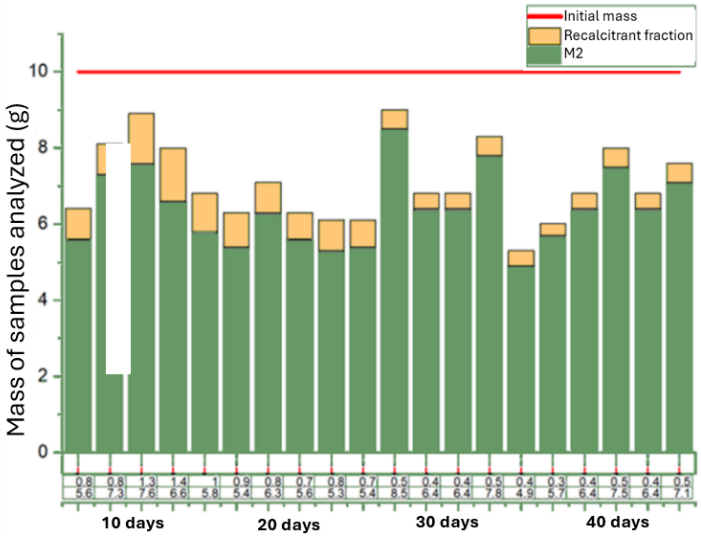


Fig. 4.27. Values of the recalcitrant fraction (C recalcitrant) and of the final litter mass for the species *Typha latifolia*

The graph in Figure 4.28 shows the proportions of active and recalcitrant C reservoirs in the litter formed by Phragmites australis. The labile fraction constitutes the largest proportion

of the TOC of the litter. Recalcitrant C, although it varies in the first phase, between days 10-30, having increased values compared to the entire series of determinations, stabilizes at constant values, representing a small percentage of the total fraction. In the first phase, recalcitrant C has values between 1.4g and 0.7g, and in the second phase of the collections, it has lower values, but with a linear trend, between 0.3g and 0.5g.

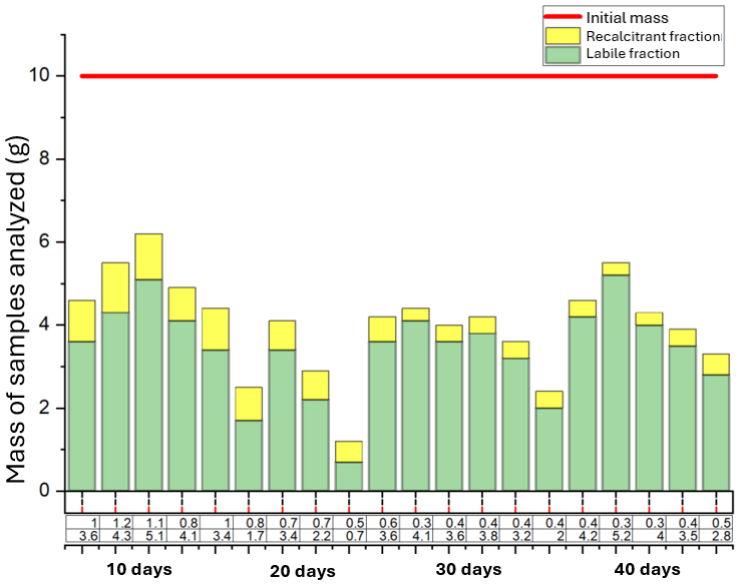


Fig. 4.28. Total organic carbon in the litter formed by the species *Typha latifolia*

Quantification of the labile fraction and the recalcitrant fraction estimated the average total mass loss of the amount of litter studied, which is composed of 2.925g active fraction and 0.675g recalcitrant fraction.

4.9.3. Estimation of carbon content in soil litter

The litter horizon is quite thin compared to the soil profile, but it contains a very high amount of OM. The determination of C_{org} from the litter horizon was performed using the estimation factor of 0.5 of the dry organic mass, proposed in previous studies [62].

Table 4.21. Carbon content of litter by components

Litter component	Carbon content for sample surfaces (kg/m2)				
	L1	L2	L3	L4	L5
Leaf	13.9 (±1.28)	12.25 (±1.32)	17.65 (±1.04)	15.47 (±0.71)	13.51 (±0.86)
Wood	2.31 (±0.13)	4.03 (±1.21)	1.61 (±2.06)	3.30 (±2.30)	2.45 (±1.54)
Total	16.21 (±5.11)	16.28 (±0.60)	19.26 (±0.93)	18.77 (±2.01)	15.96 (±0.69)

At the study area level, the litter deposited on the soil of the Dâmbovița River banks, upstream of Morii Lake, had an average content of 17.3 kg/m^2. The amount of carbon in the leaf litter presented proportions ranging between 75% and 92% of the total amount of carbon in each sample area, while wood represented percentages between 8% and 18% of the total amount of carbon (Figure 4.29).

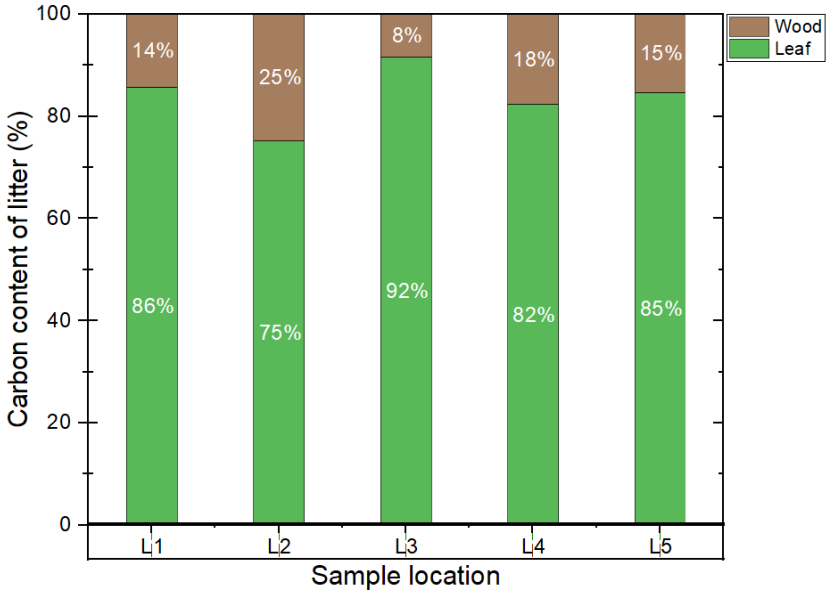


Fig. 4.29. The percentage amount of carbon on each litter component for each sample area

The amount of carbon stored in each component of the litter horizon varies quite a lot between the analyzed locations, arguing that these differences are due to intense biological activities in the soil, but also to local conditions of vegetation distribution. The carbon content of the litter is correlated with CO_2 emissions from the soil and is a direct indicator of the rate of OM mineralization. CO_2 emissions from the soil-atmosphere interface (including the litter layer) indicate an accelerated decomposition and a reduction of the stored carbon. It is recommended to expand the investigations to determine the direct correlation of the litter degradability rate and CO_2 emissions from the soil-atmosphere interface. It is important to note that the degradation of these species depends on the transformation of CO into CO_2 emissions in the atmosphere.

4.10. Assessment and forecast of CO_2 emissions using the DNDC model

To complement the analysis based on direct measurements, we used DNDC software to simulate possible evolutions of CO_2 emissions in the context of climate change. This approach allowed testing of future scenarios according to RCP 8.5 scenarios, providing insight into how climate change may influence carbon fluxes. In this way, the simulations support field measurements, providing a broader picture of emission trends in peri-urban wetlands.

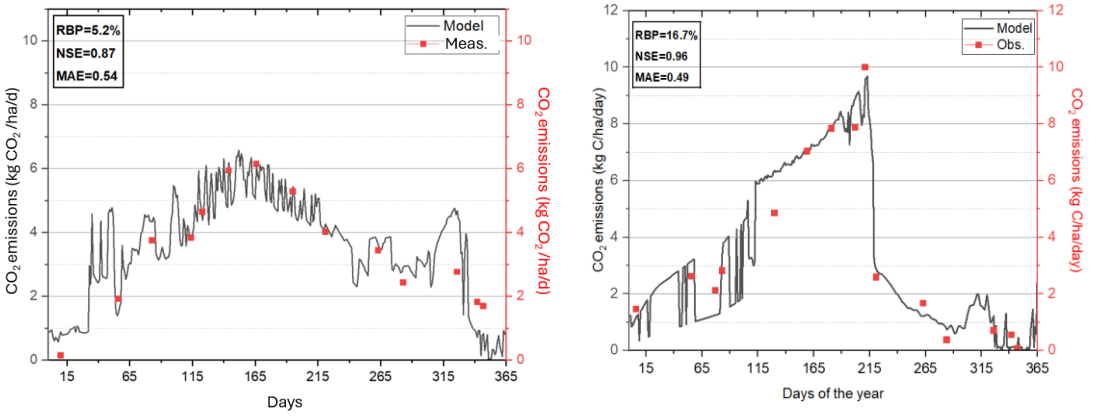
4.10.1. Validation of the DNDC model with in-situ measured data

The performance of the DNDC model was evaluated based on in-situ measurements of CO_2 emissions and performance indicators: RBP (relative weight in total error), NSE (Nash-Sutcliffe) efficiency coefficient, and MAE (mean absolute error). PBIAS (overall weight in model error) indicates whether the simulated values tend to be higher or lower than the measured data [63].

$$RBP = \frac{\Sigma_{i=1}^{n}(sim_i - ms_i)}{\Sigma_{i=1}^{n} ms_i}; NSE = 1 - \frac{\sum_{i=1}^{n} (ms_i - sim_i)^2}{\sum_{i=1}^{n}(ms_i - \overline{ms})^2}; MAE = \frac{\Sigma_{i=1}^{n}|sim_i - ms_i|}{n} \quad (4.1)$$

where sim_i represents the forecast value and ms_i represents the value obtained through in-situ measurements.

The graphs in Figure 4.30 provide a daily breakdown of CO_2 fluxes from the soil-atmosphere interface, simulated and measured for the base year 2022 in the SC (Figure 4.30 a)) and SP (Figure 4.30 b)) Locations.



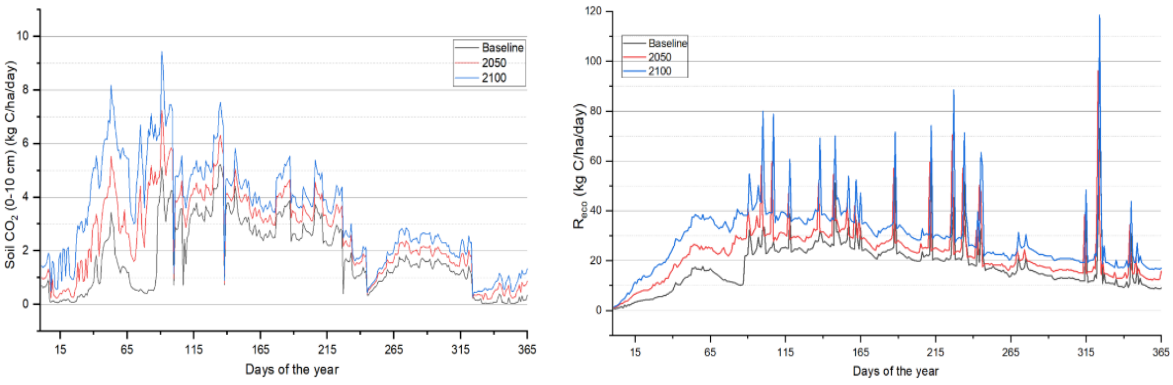
a) b)

Fig. 4.30. Interannual variations of in-situ measured and modeled soil CO_2 emissions for Location SC (a) and SP (b) in the base year [31]

The models tend to slightly overestimate CO_2 emissions compared to the measured values throughout the year; however, they are consistent with the in-situ measured data. The performance indicators show distinct differences in their predictive precision and accuracy. The SC Location has a relatively lower RBP (5.2%) compared to the SP Location (16.7%), indicating that the SC Location predictions are closer to the measured values. However, the higher NSE for the SP Location (0.96) compared to the SC Location (0.87) indicates that the SP Location model explains more of the variability in the data. Both models have roughly similar MAE values, with 0.54 for the SC Location and 0.49 for the SP Location, indicating that the average amplitude of the prediction errors is quite close.

4.10.2. CO_2 emissions forecast scenarios in the context of climate change

Under the RCP 8.5 scenario, CO_2 emissions from both locations are significantly higher in 2050 and 2100 compared to the base year values. According to Figure 4.31 a), the model for soil emissions from Location SC simulates an increase of 16.79% by 2100. Emissions for 2050 and 2100 generally follow the reference model, but with some notable differences, where the maxima in 2100 are generally higher than those in the base year and those in 2050.



a) b)

Fig. 4.31. Land surface emissions (a) and ecosystem respiration (b) simulated under RCP 8.5 scenarios for the SC Location [31]

Table 4.22 presents the greenhouse gas emissions in two different scenarios for the SC Location and the SP Location for the base year, as well as the projections for the year 2050 and the year 2100. CO_2 emissions are estimated to increase in both scenarios, for the SC Location an increase from 5960.01 kg C/ha/year at the baseline to 7215.35 kg C/ha/year by the year 2100, while for the SP Location a larger increase from 7405 kg C/ha/year at the baseline to 8443.45 kg C/ha/year by the year 2100.

Table 4.22. Model results for Location SC and Location SP and GHG emissions for each of the two scenarios (2050 and 2100 according to RCP 8.5 projection) [13]

Model Outcome		GHGs Emissions					
	Unit	SC			SP		
Scenario		Baseline	2050	2100	Baseline	2050	2100
CO_2 emissions	kgC/ha/yr	5960.01	6960.91	7215.35	7405	8091	8443.45
CH_4 emissions	kgC/ha/yr	-1.67	-1.86	-2.09	18.24	-0.42	-0.49
N_2O	kgN/ha/y	12.92	15.78	17.6	0.63	29.48	36.59
NO	kgN/ha/y	0.13	0.39	0.42	0.05	0.46	0.52
N_2	kgN/ha/y	0.41	0.9	0.99	0.12	2.68	3.2
NH_3	kgN/ha/y	22.1	36.54	38.33	53.15	59.92	66.12
*Baseline							

The simulation results indicate an increased risk of significant changes in GHG emissions by 2100, with notable variations between soil types in the analyzed wetland, according to the models.

It is recommended to calibrate the models with in-situ measurements extended over a minimum period of 3 years, in order to best capture climate and environmental variations in the locations of interest.

CHAPTER 5. GENERAL CONCLUSIONS. ORIGINAL CONTRIBUTIONS. FUTURE RESEARCH PROSPECTS. DISSEMINATION OF RESULTS.

5.1. General conclusions

Wetland ecosystems are among the most productive and significantly influence the concentration of GHG in the atmosphere. They have the capacity to sequester and store C [64], primarily through the accumulation of OM under anaerobic conditions [65]. However, wetlands also release substantial amounts of CO_2 into the atmosphere through various biogeochemical processes, contributing to GHG emissions and, implicitly, to climate change [66]. Their inclusion in national GHG inventories is essential for alignment with the IPCC Guidelines.

This doctoral thesis addresses the temporal and spatial dynamics of CO_2 emissions from the water-atmosphere interface in three areas/locations (A, B, and C) and soil-atmosphere in two locations (SC and SP), along the Dâmbovița River, upstream of Lake Morii, located in the periurban area of Bucharest, Romania. Lake Morii, completed in 1985–1986, exceeded the 25-year emission period indicated by the IPCC Guidelines, and direct measurements verified the

existence of equilibrium conditions, resulting in CO_2 emissions close to zero, which were not taken into account.

Two closed-chamber methods for point-by-point determination of CO_2 emissions from the water-atmosphere interface were used for in-situ measurements: the dynamic closed-chamber method EGM-5 and the static closed-chamber Injection Kit method. The research aimed to demonstrate the complementarity in terms of accuracy and simultaneous use of the two methods applied in this case study, considering the accuracy of the EGM-5 method as a reference for the verification of the Injection Kit method.

The results showed that the EGM-5 and Injection Kit methods are complementary in measuring CO_2 emissions [48], each performing under different conditions. The statistical analysis confirmed the high sensitivity of the EGM-5 method for high flows and the performance of the Injection Kit method for constant flows. Thus, it is recommended to use the EGM-5 method as the main method, due to its high sensitivity and the demonstrated correlation with the Injection Kit, but the simultaneous use of the two methods provides results with a high degree of accuracy and confidence in the dynamics of CO_2 emissions.

For a mutual calibration and statistical validation of the results, in the case of point measurements, it is recommended to use the regression equations presented in Table 4.6, and in the case of taking into account the shape and specificity of the analyzed area, it is recommended to apply the regression equations presented in Table. 4.7 to improve the accuracy of the interpretation of the values.

Starting from the values measured at both the water-atmosphere and soil-atmosphere interfaces, the monthly average CO_2 emissions were weighted by introducing a coefficient based on the duration of the day and night hours for each month, in order to capture intra-annual variations as realistically as possible. However, for a more comprehensive characterization of the variations, it is recommended to also take into account periods with cloudy skies, precipitation, or increased solar radiation, as these can influence CO_2 emissions [67].

Also, for CO_2 emissions from the water-atmosphere interface, the geometric shape of the investigated wetland was taken into account, and a coefficient (C_{ND}) was introduced that takes into account the ratio between the vegetation and water surface, as well as the perimeter of each area (A, B, and C). The temporal and spatial dynamics at the area level of CO_2 emissions from the water-atmosphere interface were analyzed, given the interdependence of the methods, only based on the extrapolated values at the area level for the EGM-5 method, which is based on the principle of an air collection pump, suitable for dynamic measurements. However, in situations where only measurements made with the Injection Kit method are available, it is recommended to apply the relationships presented in Table 4.13, since the statistical-mathematical models included are more general and have a high level of confidence, independent of factors such as temperature, pressure, day-night variations or the geometric particularities of the area. For the general estimation of CO_2 emissions from the water-atmosphere interface in periurban wetlands, it is recommended to use the regression equation (4.1.), which takes into account both the day-night variation and the total geometric shape and spatial distribution of vegetation.

Thus, all three areas showed clear seasonal patterns of CO_2 emissions, with the highest levels observed in summer and the lowest in winter. Area A shows the most significant increase in CO_2 emissions in summer, with greater variability than in other seasons, showing a pronounced sensitivity to temperature.

Temporal variations showed similar trends with CO_2 emissions from a wetland located in southern Finland, created for water collection [68], as well as from rivers and canals in the Danube Delta [69], where the monthly average of CO_2 emissions from the water-atmosphere interface during the peak of the growing season, from June to September, exceeded those in the remaining months.

Spatial variations are also evident between the three study areas, especially in the summer season when CO_2 emissions from Area A differ significantly from both Area B ($t=4.243$, $p=0.049$) and Area C ($t=5.767$, $p=0.029$). ANOVA analysis for all three areas confirmed the statistically significant differences between the areas ($F=23.094$, $p=0.002$).

In terms of the dependence of CO_2 emissions on the main meteorological and physical parameters, all three studied areas presented clear patterns of CO_2 emissions depending on temperatures (T_{air} and T_{soil}). The results show that at high temperatures above 25°C, biological activity intensifies, generating higher CO_2 emissions, while at minimum T_{air} and T_{soil} values, the processes are reduced and generate low CO_2 emissions. Statistical analyses reinforce these dependencies, with the Pearson coefficient correlations being significant and positive, both for T_{air} ($r=0.813$; $p<0.01$ for Area A, $r=0.857$; $p<0.01$ for Area B and $r=0.845$; $p<0.01$ for Area C) and for T_{water} ($r=0.764$; $p<0.01$ for Area A, $r=0.742$; $p<0.01$ for Area B and $r=0.894$; $p<0.01$ for Area C).

To estimate CO_2 emissions from the water-atmosphere interface according to the main dependent meteorological and physical parameters, it is recommended to use the regression equations presented in Table 4.15.

For a more precise explanation of the emissions from the water-atmosphere interface, they were analyzed in relation to the values of the water quality parameters in each study area. To estimate CO_2 emissions from the water-atmosphere interface according to these parameters, it is recommended to use the multiple regression equations presented in Table 4.18. To estimate CO_2 emissions at the general level of the area of interest, it is recommended to use equation 4.2.

Research on the analysis of CO_2 emissions from the soil-atmosphere interface from the SC and SP locations showed that the SC Location generally has higher and more constant emissions throughout the year. The seasonal emission dynamics show that emissions are lowest in winter, followed by a gradual increase in spring, reaching maximums in summer, then decreasing again in autumn. The differences between the two locations show higher averages in winter and spring, but with different variability in the SC Location, while the SP Location has lower and more stable emissions. In summer, CO_2 emissions were considerably higher in the SP Location compared to the SC Location, due to the soil flooding event, but the observed differences were not confirmed by the t-test and ANOVA analysis, which indicated a lack of statistical significance.

To estimate CO_2 emissions from the soil-atmosphere interface depending on the main parameters, it is recommended to use the regression equations presented in Table 4.16.

In terms of the dependence of CO_2 emissions on the main meteorological and physical parameters, the SC and SP Locations show notable differences. In the SC Location, CO_2 emissions increase with increasing temperatures, reaching a seasonal maximum of 22.58 g m^{-2} day^{-1} in the summer months, when T_{air} exceeds 30°C. The Pearson correlation coefficient between temperatures and CO_2 emissions is significant, with $r=0.907$; ($p<0.01$) for T_{air} and $r=0.890$; ($p<0.01$) for T_{soil}. In the SP Location, CO_2 emissions increase progressively until

August, when they reach a maximum of 37.35 g m^{-2} day^{-1}, under conditions of T_{air} above 32°C and T_{soil} of 26.9°C. The Pearson coefficient correlations between CO_2 emissions and T_{air} ($r=0.852$; $p<0.01$) and T_{soil} ($r=0.842$; $p<0.01$) are strongly positive and statistically significant. Pp (7 days) plays a major role in amplifying CO_2 emissions, with a maximum during periods of high precipitation in May and June (17-18 mm/day), and the Pearson correlation is very strong ($r=0.873$; $p<0.01$ for the SC Location and $r=0.936$; $p<0.01$ for the SP Location), indicating their importance in supporting biological processes, so that, between M_{soil} and CO_2 emissions, a positive and significant Pearson coefficient correlation results, with $r=0.829$; ($p<0.01$) for the SC Location and $r=0.871$; ($p<0.01$) for the SP Location.

Considering that starting from August, the soil in the SP Location becomes flooded, the correlations with M_{soil} up to that moment explain 84.1% of the emission variations. The maximum emission values coincide with the flood period and are due to the sudden change in the humidity regime and the disturbance of the ecosystem, which accelerated the CO_2 emissions from the soil. Subsequently, under conditions of continuous saturation, superimposed with the decrease in temperatures, the emission values showed a decreasing trend, indicating a favorable potential for CO_2 capture in the flooded soils.

To estimate CO_2 emissions from the soil-atmosphere interface depending on the main dependent meteorological and physical parameters, it is recommended to use the regression equations presented in Table 4.19 and Table 4.20. The general equation for estimating CO_2 emissions from the soil-atmosphere interface depends on the type of soil, which implies a deeper analysis in this regard.

The study also investigated how the decomposition of surface vegetation, composed of *Phragmites australis* and *Typha latifolia*, could contribute to the carbon cycle in the study area. For this, we used the litter bag method, which allowed for the direct measurement of the degradability rate under the specific conditions of the study area analyzed. Thus, the degree of litter decomposition, depending on the specific vegetation type, generally followed a pattern of degradation of the quality of the analyzed material, involving a rapid weight loss in the initial phase, followed by a slowdown in the rate of recalcitrant materials, for both *Phragmites australis* and *Typha latifolia*. By analyzing the labile and recalcitrant average fractions, the total litter mass loss was determined, being composed of 8.56% active fraction and 1.53% recalcitrant fraction for the *Phragmites australis* species and 7.31% labile fraction and 1.69% recalcitrant fraction for the *Typha latifolia* species. Thus, the results show that, although the decomposition process took place under the same environmental conditions, the *Phragmites australis* species exhibited faster decomposition.

The litter layer deposited on the soil produced an average value of 17.3 kg/m^2 C. The amount of carbon in leaf litter represented 75% to 92% of the total carbon in each sample, while the amount of carbon in wood represented 8% to 18% of the TOC. To this amount of carbon in the soil litter layer is added a contribution of plant biomass from the soil surface or from the water, depending on the hydrodynamic regime, of 14.9% from the species *Phragmites australis* and 16% from the species *Typha latifolia*. It is important to note that the transformation of CO into CO_2 emissions into the atmosphere depends on the degradation of these species.

To complement the analysis based on direct measurements, we used DNDC software to simulate possible evolutions of CO_2 emissions in the context of climate change. DNDC models for Locations SC and SP were calibrated and validated with in-situ measurements, and the performance indicators (NSE, RBP, and MAE) [70] demonstrated consistency and good

correlation with field data, which confirms their high degree of confidence for applicability in future scenarios for assessing CO_2 emissions. DNDC models according to the RCP 8.5 scenario for both locations indicate substantial increases in CO_2 emissions by 2100, compared to the base year. For Location SC, a 16.79% increase in CO_2 emissions from the land surface by 2100 was simulated, and for Location SP, a 14.02% increase was simulated. The simulation results indicate an increased risk of significant changes in GHG emissions by 2100, with notable variations between soil types in the analyzed wetland, according to the models.

It is recommended to calibrate the models with in-situ measurements extended over a minimum period of 3 years, in order to best capture climate and environmental variations in the locations of interest.

5.2. Original contributions

1. This research on CO_2 emissions from wetlands contributes to improving the information volume needed for national GHG inventories by providing high-confidence data, in line with IPCC requirements, essential for LULUCF sector reporting.

2. Two complementary methods, the closed dynamic chamber method (EGM-5) and the static chamber method with the Injection Kit, were tested and validated, demonstrating that their simultaneous use provides greater confidence in measurements, especially in peri-urban wetland ecosystems that have not been investigated to date.

3. Through statistical analyses, parameters such as air and soil temperature, $M_{soil,}$ and pH were highlighted as the main factors controlling CO_2 emissions, confirming the interdependence of physico-chemical and biological processes in peri-urban wetland ecosystems.

4. In the locations studied for CO_2 emissions from the soil-atmosphere interface, the hydrological regime (flooding) had a major influence on the dynamics of emissions, demonstrating that flash flooding accelerates anaerobic decomposition processes and, implicitly, the increase in CO_2 emissions from peri-urban wetlands.

5. Extrapolation of CO_2 emissions based on in-situ measurements, including diurnal and nocturnal variations, was used for the first time in this study and provides a more detailed picture of the flux at the seasonal level

6. Development of a CO_2 emission estimation coefficient (CND), which explains the variations depending on the geometric shape of the area and the spatial distribution of vegetation.

7. Extrapolation of CO_2 emissions based on in-situ measurements, including the ratio between the vegetation surface and the water surface and the geometric shape, was used for the first time in this study and provides a more detailed picture of the flux at the area level.

8. The use of statistical-mathematical models allowed the development of predictive models for CO_2 emissions from the soil-atmosphere interface, which explain the variations of emissions at the area level, depending on meteorological and physico-chemical parameters, being a valuable tool for future climate scenarios used for the first time for this purpose.

9. Development of a general model for estimating CO_2 emissions from the water-atmosphere interface in peri-urban wetlands, which considers both day-night variation and the overall geometric shape and spatial distribution of vegetation.

10. Development of a general model for estimating CO_2 emissions from the water-atmosphere interface in peri-urban wetlands, which considers both day-night variation and the overall geometric shape and spatial distribution of vegetation.

11. Validation of predictive models developed in DNDC software, by analyzing model performance and uncertainties by comparing with data obtained through direct measurements

12. Development of a general model for estimating CO_2 emissions from the soil-atmosphere interface in peri-urban wetlands, which takes into account meteorological and physical soil parameters

13. Creation of models based on future climate conditions, using RCP8.5 scenarios, was used to assess how climate change may influence emissions from urban wetlands

14. The high-confidence data and models developed and validated in the presented research are designed by the author and ensure greater precision in CO_2 emission estimates.

15. The results and methods developed in this doctoral thesis, which focused on the assessment of CO_2 emissions in urban wetlands, provide important support for the application of NbS in cities, with the aim of adapting them to climate change

16. Presentation of a replicable methodology at the national level for monitoring peri-urban wetlands

17. Analysis of wetland soils according to the water regime and determination of emission differences depending on the degree of flooding and the hydrological characteristics of the soil.

18. Combined application of the EGM-5 method and the Injection Kit for in-situ monitoring of CO_2 emissions in wetlands and a detailed comparative analysis of seasonal variations

9. By developing the patent entitled ”Device for direct determination of gas flows (especially greenhouse gases) in a submerged chamber drained from the substrates of aquatic ecosystems (mud, silt, sediments, etc.), a significant contribution is ensured in estimating CO_2 emissions in wetlands that significantly contribute to future reports on national GHG inventories.

20. By developing the patent “Technology based on artificial intelligence for evaluating performance in organic agriculture and reducing greenhouse gas emissions”, an innovative AI-based technology is proposed that simultaneously analyzes soil and climate data, with direct relevance for reducing GHG emissions and land management in the context of climate change.

5.3. Future research perspectives

This doctoral thesis aimed to assess CO_2 emissions from peri-urban wetland ecosystems, but a more elaborate accounting of the GHG balance requires the quantification of CH_4 and N_2O (nitrous oxide), gases with a much higher warming potential.

Also, extending the monitoring period of CO_2 emissions represents a direction for future research, since a data series extended to at least 3 years would allow capturing interannual variations and would provide a more complex picture of CO_2 emission trends.

Another important aspect for future research is the analysis of how meteorological parameters, such as the degree of cloudiness and the level of solar radiation, influence CO_2 emissions.

Further investigation is recommended to determine the direct correlation between litter degradability rate and CO_2 emissions from the soil-atmosphere interface.

A future research direction is to adapt and calibrate the DNDC model to the specific pedoclimatic conditions of the region. This would reduce the uncertainties in GHG flux predictions, facilitating the integration of the results into national-scale assessments.

BIBLIOGRAPHY

[1] *Intergovernmental Panel on Climate Change (IPCC), SAR Climate Change 1995: The Science of Climate Change*, Cambridge University Press, 2024.

[2] N. Faivre, M. Fritz, T. Freitas, B. de Boissezon, S. Vandewoestijne*, Nature-Based Solutions in the EU: Innovating with nature to address social, economic and environmental challenges*, *Environmental Research*, vol. **159**, nov. 2017, pp. 509–518. doi: 10.1016/j.envres.2017.08.032.

[3] W. J. Mitsch, J. G. Gosselink, *Wetlands*, 5th Edition, John Wiley & Sons, Inc., Hoboken, 2015.

[4] Intergovernmental Panel on Climate Change (IPCC), *Climate Change 2014: Synthesis Report. Contribution of Working Groups I, II and III to the Fifth Assessment Report of the Intergovernmental Panel on Climate Change*, Geneva, Elveția: IPCC, 2014.

[5] A. Zuazua Ruiz, J. M. Martín Martín, J. F. Prados-Castillo, *The European Union facing climate change: a window of opportunity for technological development and entrepreneurship*, *Sustainable Technology and Entrepreneurship*, **vol. 2**, nr. 2, 2023, 100035. ISSN 2773-0328. doi: 10.1016/j.stae.2022.100035.

[6] United Nations Framework Convention on Climate Change (UNFCCC), *United Nations Framework Convention on Climate Change*, New York, 1992.

[7] M. Grubb, *Kyoto and the Future of International Climate Change Responses: From Here to Where*, *International Review for Environmental Strategies*, **vol. 5**, 2004, pp. 15–38.

[8] M. Voicu, V. Coman, N. Enache, L. Laslo, M. Matei, A. Rotaru, N. Bara, M. Boboc, S. Stanciu, G. Deak*, Experimental Determination of Carbon Dioxide Flux in Soil and Correlation with Dependent Parameters, IOP Conference Series: Earth and Environmental Science*, vol. **616,** 012010, 2020. doi: 10.1088/1755-1315/616/1/012010.

[9] H. Böttcher, J. Reise, *The Climate Impact of Forest and Land Management in the EU and the Role of Current Reporting and Accounting Rules*, Öko Institut, Berlin, Germania, 2020.

[10] R. Petrescu, G. Peters, G. Janssens-Maenhout, P. Ciais, F. Tubiello, G. Grassi, G. Nabuurs, A. Leip, G. Carmona Garcia, W. Winiwarter, L. Höglund-Isaksson, D. Gunther, E. Solazzo, A. Kiesow, A. Bastos, J. Pongratz, J. Nabel, G. Conchedda, R. Pilli, R. Andrew, M. Schelhaas, A. Dolman, *European anthropogenic AFOLU greenhouse gas emissions: a review and benchmark data*, *Earth System Science Data*, vol. 12, nr. 2, 2020, pp. 961–1001. JRC118629. doi: 10.5194/essd-12-961-2020.

[11] Intergovernmental Panel on Climate Change (IPCC), *2019 Refinement to the 2006 IPCC Guidelines for National Greenhouse Gas Inventories*, E. Calvo Buendia, K. Tanabe, A. Kranjc, J. Baasansuren, M. Fukuda, S. Ngarize, R. Osako, Y. Pyrozhenko, P. Shermanau, S. Federici (eds.), Geneva, Elveția: IPCC, 2019.

[12] Parlamentul European și Consiliul Uniunii Europene, *Regulamentul (UE) 2018/841 al Parlamentului European și al Consiliului din 30 mai 2018 privind includerea emisiilor și absorbțiilor de gaze cu efect de seră rezultate din utilizarea terenurilor, schimbarea utilizării terenurilor și silvicultură în cadrul de acțiune privind clima și energia pentru 2030 și de modificare a Regulamentului (UE) nr. 525/2013 și a Deciziei nr. 529/2013/UE*, *Jurnalul Oficial al Uniunii Europene*, L156, 2018.

[13] N. Enache, G. Deák, L. Laslo, M. Matei, E. Holban, M. Boboc, A. Harabagiu, *Modelling the impact of soil and meteorological parameters on carbon dynamics in wetland ecosystems*, *International Journal of Conservation Science*, **vol. 15**, nr. 3, 2024, pp. 1523–1532. doi: 10.36868/IJCS.2024.03.23.

[14] B. Arora, N. F. Spycher, C. I. Steefel, S. Molins, M. Bill, M. E. Conrad, W. Dong, B. Faybishenko, T. K. Tokunaga, J. Wan, K. H. Williams, S. B. Yabusaki, *Influence of hydrological,*

biogeochemical and temperature transients on subsurface carbon fluxes in a flood plain environment, *Biogeochemistry*, **vol. 127**, 2016, pp. 367–396. doi: 10.1007/s10533-016-0186-8.

[15] K. W. Krauss, J. L. Whitbeck, R. J. Howard, *On the relative roles of hydrology, salinity, temperature, and root productivity in controlling soil respiration from coastal swamps (freshwater)*, *Plant and Soil*, **vol. 358**, 2012, pp. 265–274. doi: 10.1007/s11104-012-1182-y.

[16] K. Guan, S. Thompson, C. Harman, N. Basu, P. S. C. Rao, M. Sivapalan, A. I. Packman, P. Kalita, *Spatiotemporal Scaling of Hydrological and Agrochemical Export Dynamics in a Tile-Drained Midwestern Watershed*, *Water Resources Research*, **vol. 47**, 2011. doi: 10.1029/2010WR009997.

[17] J. Hassink, *Effects of soil texture and structure on carbon and nitrogen mineralization in grassland soils, Biology and Fertility of Soils*, **vol. 14**, 1992, pp. 126–134. doi: 10.1007/BF00336262.

[18] K. R. Reddy, R. D. DeLaune, *Biogeochemistry of Wetlands: Science and Applications*, 1st ed., Boca Raton: CRC Press, 2008. doi: 10.1201/9780203491454.

[19] L. Olsson, S. Ye, X. Yu, M. Wei, K. W. Krauss, H. Brix, *Factors influencing CO_2 and CH_4 emissions from coastal wetlands in the Liaohe Delta, Northeast China*, *Biogeosciences*, **vol. 12**, 2015, pp. 4965–4977. doi: 10.5194/bg-12-4965-2015.

[20] K. Tockner, J. A. Stanford, *Riverine Flood Plains: Present State and Future Trends*, *Environmental Conservation*, **vol. 29**, nr. 3, 2002, pp. 308–330. doi: 10.1017/S037689290200022X.

[21] Gy. Deák, N. Enache, L. Laslo, M. Matei, M. G. Boboc, C. I. Covaliu Mierla, *Water CO_2 Emission Monitoring in a Romanian Peri-Urban Wetland to Enhance GHG Reporting*, *Atmosphere*, **vol. 15**, nr. 11, 2024, p. 1345. doi: 10.3390/atmos15111345.

[22] E. A. Davidson, I. A. Janssens, *Temperature Sensitivity of Soil Carbon Decomposition and Feedback to Climate Change*, *Nature*, **vol. 440**, 2006, pp. 165–173. doi: 10.1038/nature04514.

[23] L. Laslo, N. Enache, M. Matei, M. Boboc, A. Radu, N. Ramli, *Experiments on Soil Microcosms for the Assessment of Greenhouse Gases Fluxes from Different Land Uses in Laboratory Conditions*, *E3S Web of Conferences*, **vol. 589**, 2024, p. 01005. doi: 10.1051/e3sconf/202458901005.

[24] S. Kakran, J. S. Rathore, A. Sidhu, A. Kumar, *Solar energy advances and CO_2 emissions: A comparative review of leading nations' path to sustainable future*, *Journal of Cleaner Production*, **vol. 475**, 2024, p. 143598. doi: 10.1016/j.jclepro.2024.143598.

[25] O. K. Atkin, M. G. Tjoelker, *Thermal acclimation and the dynamic response of plant respiration to temperature*, *Trends in Plant Science*, **vol. 8**, nr. 7, 2003, pp. 343–351. doi: 10.1016/S1360-1385(03)00136-5.

[26] M. E. Dusenge, A. G. Duarte, D. A. Way, *Plant carbon metabolism and climate change: elevated CO_2 and temperature impacts on photosynthesis, photorespiration and respiration*, *New Phytologist*, **vol. 221**, nr. 1, 2019, pp. 32–49. doi: 10.1111/nph.15283.

[27] Z. Yang, K. Chen, F. Liu, Z. Che, *Effects of Rainfall on the Characteristics of Soil Greenhouse Gas Emissions in the Wetland of Qinghai Lake*, *Atmosphere*, **vol. 13**, nr. 1, 2022, art. 129. doi: 10.3390/atmos13010129.

[28] J. Tang, D. D. Baldocchi, Y. Qi, L. Xu, *Assessing soil CO_2 efflux using continuous measurements of CO_2 profiles in soils with small solid-state sensors*, *Agricultural and Forest Meteorology*, **vol. 118**, nr. 3–4, 2003, pp. 207–220.

[29] S. M. Green, R. Machin, M. S. Cresser, *Long-term impacts of atmospheric deposition on peatland soils and vegetation: A synthesis*, *Ecology Letters*, **vol. 14**, nr. 10, 2011, pp. 1104–1116.

[30] W. Zhang, M. Wang, X. Zhu, *Plant-mediated influences of wind on soil CO_2 flux in wetland ecosystems*, *Ecological Applications*, **vol. 27**, nr. 4, 2017, pp. 1251–1260.

[31] L. Laslo, N. Enache, A. Rotaru, N. Bara, Gy. Deák, M. Matei, M. Boboc, *Improving the efficiency to measure the aquatic and terrestrial exchange of greenhouse gases by using static chambers and injection methods*, *RA Journal of Applied Research*, 2021.

[32] Y. Luo, S. Wan, D. Hui, L. L. Wallace, *Acclimatization of soil respiration to warming in a tall grass prairie*, *Nature*, **vol. 413**, nr. 6856, 2001, pp. 622–625. https://doi.org/10.1038/35098065

[33] G. J. Whiting, J. P. Chanton, *Greenhouse carbon balance of wetlands: Methane emission versus carbon sequestration*, *Biogeochemistry*, **vol. 15**, nr. 2, 2001, pp. 135–161. https://doi.org/10.1007/BF00002932

[34] R. J. Diaz, R. Rosenberg, *Spreading dead zones and consequences for marine ecosystems*, *Science*, **vol. 321**, nr. 5891, 2008, pp. 926–929. https://doi.org/10.1126/science.1154122

[35] R. G. Wetzel, *Limnology: Lake and River Ecosystems* (3rd ed.), Academic Press, 2001. https://doi.org/10.1002/9780470999271

[36] R. Conrad, *The global methane cycle: Recent advances in understanding the microbial processes involved*, *Environmental Microbiology Reports*, **vol. 1**, nr. 5, 2009, pp. 285–292. https://doi.org/10.1111/j.1758-2229.2009.00038.x

[37] R. G. Wetzel, *Limnology: Lake and River Ecosystems* (3rd ed.), Academic Press, 2001. https://doi.org/10.1002/9780470999271

[38] N. Fenner, C. Freeman, *Drought-induced C loss in peatlands*, *Nature Geoscience*, **vol. 4**, 2011, pp. 895–900. doi: 10.1038/ngeo1323.

[39] T. R. Moore, N. Basiliko, *Decomposition in boreal peatlands*, in *Soil Processes and Water Quality*, **vol. 1**, nr. 6, 2006, pp. 125–143. https://doi.org/10.1007/978-94-017-3356-3_8

[40] P. M. Vitousek, R. Naylor, T. Crews, J. J. Dighton, *Nutrient imbalances in agricultural development*, *Science*, **vol. 324**, nr. 5934, 2010, pp. 1519–1520. https://doi.org/10.1126/science.117026

[41] A. Kuznetsova, A. E. Kazakova, E. I. Alekseeva, *Impact of eutrophication on carbon balance in wetlands*, *Wetlands Ecology and Management*, **vol. 18**, nr. 6, 2010, pp. 675–685. https://doi.org/10.1007/s11273-010-9192-2

[42] K. Anderson, K. J. Gaston, *Lightweight unmanned aerial vehicles will revolutionize spatial ecology, Frontiers in Ecology and the Environment*, **vol. 11**, nr. 3, 2013, pp. 138–146. DOI: 10.1890/120150.

[43] *Ecopolis. Raport: Starea mediului în regiunea București-Ilfov*, 2022.

[44] *Meteoblue.* Meteoblue Weather Service. Disponibil online: www.meteoblue.com

[45] *Climate Analytics.* Disponibil online: www.climateanalytics.org

[46] PP Systems, *EGM-5 Portable CO_2 Gas Analyzer: User Manual*

[47] L. Laslo, M. Matei, M. Boboc, Gy. Deák, I. Cătuneanu, N. Enache, *Measurements and Statistical Analysis of CO_2 Efflux and Related Parameters from Crop and Forested Lands*, IOP Conference Series: Earth and Environmental Science, 2023.

[48] Gy. Deák, A. Rotaru, N. A. Enache, L. Laslo, M. Matei, M. Boboc, N. Bara, *Carbon Dioxide Sampling and Analysis Technologies for Aquatic and Terrestrial Ecosystems*, *ECS Transactions*, **vol. 107**, 2022, pp. 6525–6540. doi: 10.1149/10701.6525ecst.

[49] C. Draghici, I. Manciulea, *Calitatea mediului: Monitorizarea solului (Unitatea 3, Modulul 6.4)*, Brașov, România: Universitatea Transilvania din Brașov, 2015.

[50] E. Grüneberg, D. Ziche, N. Wellbrock, *Organic Carbon Stocks and Sequestration Rates of Forest Soils in Germany*, Global Change Biology, **20**(8), 2014, pp. 2644–2662. https://doi.org/10.1111/gcb.12558

[51] B. L. Vasilias, M. Rabenhorst, J. Fuhrmann, A. Chirnside, S. Inamdar, în: J. T. Anderson, C. A. Davis (eds.), *Wetland Techniques. Volume 1: Foundations*, New York, NY: Springer, 2013, pp. 355–442.

[52] G. S. Deghi, K. C. Ewel, W. J. Mitsch, *Effects of Sewage Effluent Application on Litter Fall and Litter Decomposition in Cypress Swamps*, Journal of Applied Ecology, **17**, 1980, pp. 397–408.

[53] S. M. Vargo, R. K. Neely, S. M. Kirkwood, *Emergent Plant Decomposition and Sedimentation: Response to Sediments Varying in Texture, Phosphorus Content and Frequency of Deposition*, Environmental and Experimental Botany, **40**, 1998, pp. 43–58.

[54] E. F. Benfield, în: F. R. Hauer, G. A. Lamberti (eds.), *Methods in Stream Ecology*, San Diego, CA: Academic Press, 1996, pp. 579–589.

[55] J. Morris, K. Lajtha, *Decomposition and Nutrient Dynamics of Litter from Four Species of Freshwater Emergent Macrophytes*, Hydrobiologia, **131**, 1986, pp. 215–223.

[56] *IBM Corp.*, *IBM SPSS Statistics for Windows, Version 29.0.* Armonk, NY: IBM Corp., 2021.

[57] *OriginLab, OriginPro 2023: Data Analysis and Graphing Software.* Northampton, MA: OriginLab Corporation, 2023.

[58] https://www.dndc.sr.unh.edu

[59] Cohen, *Statistical Power Analysis for the Behavioural Sciences*, 2nd ed.; Lawrence Erlbaum Associates, Hillsdale, NJ, USA, 1988.

[60] N. Enache, L. Laslo, M. Matei, M. Boboc, I. Cătuneanu, G. Deák, *Analysis of the Results from the Applied Technologies for Carbon Dioxide Sampling in Aquatic Ecosystems*, IOP Conf. Ser.: Earth Environ. Sci., **1216**, 012006, 2023. https://doi.org/10.1088/1755-1315/1216/1/012006

[61] N. Enache, G. Deák, C. I. Covaliu-Mierlă, L. Laslo, M. Matei, M. Boboc, S. Stegarescu, L. Bugeac, D. Zaharia, *Carbon Content Estimation in an Aquatic Ecosystem Case Study through the Process of Leaf Litter Decomposition*, U.P.B. Sci. Bull., Series B, **86**(4), 2024.

[62] C. Akselsson, B. Berg, V. Meentemeyer, O. Westling, *Carbon Sequestration Rates in Organic Layers of Boreal and Temperate Forest Soils — Sweden as a Case Study*, Global Ecology and Biogeography, **14**, 2005, pp. 77–84. https://doi.org/10.1111/j.1466-822X.2004.00133.x

[63] D. N. Moriasi, M. W. Gitau, N. Pai, P. Daggupati, *Hydrologic and Water Quality Models: Performance Measures and Evaluation Criteria*, Transactions of the ASABE, **58**(6), 2015, pp. 1763–1785. https://doi.org/10.13031/trans.58.10715

[64] W. R. Moomaw, G. L. Chmura, G. T. Davies, et al., *Wetlands in a Changing Climate: Science, Policy and Management*, Wetlands, **38**, 2018, pp. 183–205. https://doi.org/10.1007/s13157-018-1023-8

[65] Y. Zhang, X. Zhang, W. Fang, Y. Cai, G. Zhang, J. Liang, J. Chang, L. Chen, H. Wang, P. Zhang, Q. Wang, Y. Zhang, *Carbon Sequestration Potential of Wetlands and Regulating Strategies Response to Climate Change*, Environmental Research, **269**, 2025, p. 120890. https://doi.org/10.1016/j.envres.2025.120890

[66] A. Pradhan, A. Sao, T. K. Thakur, J. T. Anderson, G. Chandel, A. Kumar, V. Paramesh, D. Jinger, R. Kumar, *Wetlands as Climate-Sensitive Hotspots: Evaluating Greenhouse Gas Emissions in Southern Chhattisgarh*, Water, **17**(10), 2025, p. 1553. https://doi.org/10.3390/w17101553

[67] K. Zhang, Y. Wang, A. Mamtimin, Y. Liu, *Variation Characteristics and Influencing Mechanisms of CO_2 Flux from Grassland Ecosystem in the Central Tianshan Mountains, China*, Ecological Indicators, **170**, 2025, p. 113069. https://doi.org/10.1016/j.ecolind.2024.113069

[68] X. Li, O. Wahlroos, S. Haapanala, J. Pumpanen, H. Vasander, A. Ojala, T. Vesala, I. Mammarella, *Carbon Dioxide and Methane Fluxes from Different Surface Types in a Created Urban Wetland*, Biogeosciences, **17**, 2020, pp. 3409–3425.

[69] M.S. Maier, C. R. Teodoru, B. Wehrli, *Spatio-Temporal Variations in Lateral and Atmospheric Carbon Fluxes from the Advantages of the Mean Absolute Error*, Biogeosciences, **18**, 2021, pp. 1417–1437.

[70] C. J. Willmott, K. Matsuura, *Advantages of the Mean Absolute Error (MAE) over the Root Mean Square Error (RMSE) in Assessing Average Model Performance*, Climate Research, **30**(1), 2005, pp. 79–82. https://doi.org/10.3354/cr030079